Memory kernel and divisibility of Gaussian collisional models

Rolando Ramirez Camasca [*] and Gabriel T. Landi [†]
Instituto de Física da Universidade de São Paulo, 05314-970 São Paulo, Brazil

(Received 10 August 2020; revised 21 October 2020; accepted 22 December 2020; published 3 February 2021)

Memory effects in the dynamics of open systems have been the subject of significant interest in the last decades. The methods involved in quantifying this effect, however, are often difficult to compute and may lack analytical insight. With this in mind, we study collisional models where non-Markovianity is introduced by means of additional interactions between neighboring environmental units. We show that the dynamics can be cast in terms of a Markovian embedding of the covariance matrix, which yields closed-form expressions for the memory kernel that governs the dynamics, a quantity that can seldom be computed analytically. The same is also possible for a divisibility monotone, based on the complete positivity of intermediate maps. By focusing on continuous-variable Gaussian dynamics, we are able to analytically study models of arbitrary size. We analyze in detail two types of interactions, a beam splitter implementing a partial SWAP and a two-mode squeezing, which entangles the ancillas and, at the same time, feeds excitations into the system. By analyzing the memory kernel and divisibility for these two representative scenarios, our results help to shed light on the intricate mechanisms behind memory effects in the quantum domain.

DOI: 10.1103/PhysRevA.103.022202

I. INTRODUCTION

The growing interest in quantum information processing applications has highlighted the need for furthering our knowledge on the notion of *information flow*. Unlike classical systems, in the quantum realm information leaks are much more efficient, so that when a system interacts with an environment, information about the former is inevitably transferred to the latter. When the environment is very large and complex, this information may never return. In this case the dynamics is called Markovian. In general, however, there may be a partial backflow of information, which characterizes a non-Markovian evolution [1]. From the point of view of causality, this backflow quantifies the ability of the dynamics to communicate past information to the future [2]. Non-Markovianity therefore touches at the core of information processing, which justifies the need for detailed studies.

Considerable attention was given in recent years on how to characterize and quantify non-Markovianity in the quantum domain (see Refs. [3,4] for two recent reviews). Due to the richness involved, however, there is no single approach capable of capturing its full essence. The most important notion is that of map divisibility: non-Markovianity requires that the underlying dynamical map should not be divisible [5,6]. The notion of information flow, on the other hand, relies on information-theoretic quantifiers and is thus not uniquely defined. The most widely used measures involve the trace distance [5–8] between different initial states or entanglement [9] between the system and an ancilla. Several other quantifiers have also been explored [10–18].

A much older notion of non-Markovianity is that of a memory kernel, as present already in the seminal works of Nakajima [19] and Zwanzig [20]. The basic idea is that the open dynamics of a system's density matrix ρ_S can, quite generally, be written as

$$\frac{d\rho_S}{dt} = -i[H_S, \rho_S] + \int_0^t \mathcal{K}_{t-t'}[\rho(t')]\, dt', \tag{1}$$

where $\mathcal{K}_{t-t'}$, called the memory kernel (MK), is a linear superoperator condensing all the information on how the evolution of ρ at time t depends on its past values. The MK has been studied intensively in recent years [21–26], as it provides clear insights onto the inner workings of non-Markovianity. It can also be given an operational interpretation, in terms of the so-called transfer tensors [27], rendering it accessible to experiments [28]. However, being a superoperator, it is generally difficult to compute it analytically. We also mention in passing the broader notion of a process tensor, which includes also all possible input and output operations performed in the system [29–31].

Analyzing non-Markovianity for general environments is in general an extremely difficult task. First, the calculations quickly become impractical when the size of the bath is large. And second, realistic baths often have many additional features which tend to mask the effects one is interested in. This motivates the search for controllable models, where the degree of non-Markovianity can be finely tuned. One way to accomplish this, which has seen an enormous surge in popularity in recent years, is through the so-called collisional models [32–43]. The basic idea is to replace the open dynamics of a system by a series of sequential interactions between the system (S) and small environmental units $E_1, E_2, E_3 \ldots$ (henceforth referred to as ancillas). All ancillas are prepared in the same state and each interaction only lasts for a fixed time,

[*] rcamasca@if.usp.br
[†] gtlandi@if.usp.br

 ©2021 American Physical Society

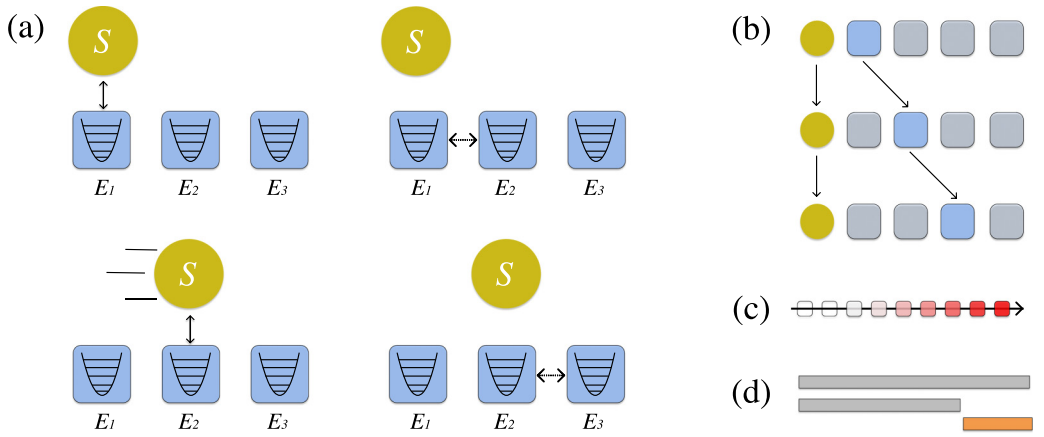

FIG. 1. Non-Markovian collisional models. (a) First few steps of the dynamics. The system-ancilla interactions SE_n are interspersed by ancilla-ancilla interactions E_nE_{n+1}, which propagate information forward, making the dynamics non-Markovian in a fully controllable way. (b) Basic structure of the Markovian embedding dynamics (24), which is a map from the Hilbert space of SE_n to that of SE_{n+1}. (c) The memory kernel [Eq. (1)] quantifies how different instants of the past affect the evolution at present times. (d) Completely positive divisibility. The maps in gray from time zero to t_n or t_m are, by construction, completely positive trace preserving. But the intermediate map from t_n to $t_m > t_n$ may not necessarily be.

after which they never interact again. This therefore leads to a stroboscopic dynamics for the system.

The advantage of collisional models is that non-Markovianity can be introduced in a fully controllable manner. There are two main ways to do so. The first is to consider that the ancillas already start correlated [44–48]. The other one is to assume information is transmitted between them during the process [49–57]. Here we shall focus on the second case. That is, we consider a scenario where neighboring ancillas E_nE_{n+1} interact with each other in between the interactions SE_n and SE_{n+1} [see Fig. 1(a)]. This additional interaction *signals* information from the past to the future, so that when the SE_{n+1} interaction arrives, the ancilla E_{n+1} will already contain some information about the system.

In this paper we overcome these difficulties by focusing on continuous-variable collisional models, undergoing Gaussian-preserving dynamics [58–66]. The advantages that come with the Gaussian toolbox allow us to construct a complete framework for the study of non-Markovianity, which (i) encompasses a broad range of scenarios, (ii) allows for the explicit construction and computation of the memory kernel, and (iii) provides easy access to a completely positive (CP) divisibility monotone, which can be directly compared with the memory kernel. The framework is also amenable to analytical calculations and extremely efficient from a numerical perspective. Thus, despite being restricted to Gaussian interactions, it offers multiple advantages over more general maps. We also provide a complete numerical library for efficiently simulating Gaussian collisional models in PYTHON [67]. All plots in this paper were generated with this code.

The paper is divided as follows. The general framework is developed in Sec. II, where we show that the full non-Markovian dynamics can be cast as a Markovian embedding, involving a Markovian map at a higher dimension [Fig. 1(b)]. We then show how all relevant quantifiers of non-Markovianity can be cast in terms of this embedding. In Sec. III we then specialize this to the case of Gaussian models, where the embedding is written as a set of matrix-difference equations with clear physical interpretation. Armed with this result, we then provide a full characterization of both the memory kernel (Sec. IV) and the map divisibility (Sec. V). Throughout the paper, our exposition will be example oriented, with a focus on two specific types of interactions. The framework, however, is general and we will specify, in each part, how to properly make this generalization.

II. FORMAL FRAMEWORK

In this section we put forth the mathematical framework for describing non-Markovian collisional models. The main result is the construction of a Markovian embedding, which converts the problem into a fully Markovian dynamics at a larger space. We then move on to show how all relevant quantifiers of non-Markovianity can be expressed in terms of this Markovian embedding. The results in this section are general: they hold for arbitrary system and bath dimensions and arbitrary interactions. However, as will be discussed, generality comes at the cost of physical insight. For this reason, in Sec. III we then specialize them to Gaussian models, which, as we show, provides significant advantages. The connection between collisional models and experimentally relevant systems is drawn in Sec. VI C and a comparison between collisional models and the more traditional approaches for open quantum dynamics is provided in Sec. VI D.

A. Non-Markovian collisional models

We consider here the collisional model scenario presented in Fig. 1. A system S is set to interact sequentially with an arbitrary number of environment ancillas $E_1, E_2, E_3, \ldots$. The ancillas are independent and identically prepared, each with initial density matrix ρ_E. The interaction between S and E_n is described by a unitary U_n. After this, S and E_n never interact again. If U_n was the only interaction involved, the dynamics would be Markovian by construction.

Here we make it non-Markovian in a controllable way, by introducing ancilla-ancilla collisions [49–56]. That is, after collision SE_n, but before SE_{n+1}, we set E_nE_{n+1} to interact with each other by means of another unitary $V_{n,n+1}$. Since E_n already interacted with S, it contains some information about it, which is then transmitted to E_{n+1} via $V_{n,n+1}$. As a consequence, when the collision SE_{n+1} starts, they will already contain some information about each other, obtained from E_n. Past information about S can thus *backflow* at SE_{n+1}, making the dynamics non-Markovian. This construction therefore provides a clean and controllable way of introducing non-Markovianity. In particular, by assuming that E_n only interacts with its neighbor E_{n+1}, we fix the memory length of the process. Collisional models with long-range interactions were discussed in Ref. [52].

Let $\rho^0 = \rho_S \otimes \rho_{E_1} \otimes \rho_{E_2} \otimes \dots$ denote the initial state of the composite system $SE_1E_2\dots$. We count time in integer steps, such that at time n the collisions SE_n and E_nE_{n+1} already took place. That is, at time n the system has already interacted with its corresponding ancilla E_n *and* this ancilla has already passed down its information to the next one. The map taking the composite system $SE_1E_2\dots$ from $n-1$ to n therefore reads

$$\rho^n = V_{n,n+1}U_n\ \rho^{n-1}\ U_n^\dagger V_{n,n+1}^\dagger. \tag{2}$$

To avoid confusion we henceforth use superscripts to denote time so that ρ^n refers to the global state of $SE_1E_2\dots$ at time n. The map (2) involves only SE_nE_{n+1}. All ancillas E_m with $m \geqslant n+2$ did not yet participate in the process and therefore remain in a product state with everything else. In addition, the ancillas with $m < n$ will never participate again and hence can be traced out (discarded). The process (2) can thus be equivalently written as

$$\rho^n_{SE_nE_{n+1}} = V_{n,n+1}U_n\ \left(\rho^{n-1}_{SE_n} \otimes \rho_{E_{n+1}}\right)\ U_n^\dagger V_{n,n+1}^\dagger, \tag{3}$$

where $\rho^{n-1}_{SE_n}$ is the state of SE_n at time $n-1$ and $\rho_{E_{n+1}} = \rho_E$, refers to the initial state of E_{n+1}. This also holds for the first step, provided one recalls that $\rho^0_{SE_1} = \rho^0_S \otimes \rho_{E_1}$. After the interaction (3), one may trace out E_n, leading to

$$\rho^n_{SE_{n+1}} = \mathrm{tr}_{E_n}\left\{V_{n,n+1}U_n\ \left(\rho^{n-1}_{SE_n} \otimes \rho_E\right)\ U_n^\dagger V_{n,n+1}^\dagger\right\} := \Phi\left(\rho^{n-1}_{SE_n}\right). \tag{4}$$

This can now be fed again to Eq. (3), to evolve to the next step. This equation also defines the quantum channel $\Phi(\cdot)$, which is a map from the Hilbert space of SE_n to that of SE_{n+1}, as depicted in Fig. 1(b). Moreover, since we are assuming that the unitaries U_n and $V_{n,n+1}$ are the same for all collisions, the map Φ, itself, is actually independent of n; the only n dependence is in the input $\rho^{n-1}_{SE_n}$.

Crucially, we see that the map $\Phi(\cdot)$ is both time local and CP, since it is written as a Stinespring dilation. Hence, it represents an entirely Markovian evolution. Equation (4) is known as a Markovian embedding of the non-Markovian dynamics [54]: It expresses a non-Markovian evolution as a Markovian one, at the expense of working with maps that act between different Hilbert spaces and also have a larger dimension.

It is convenient to define the more compact notation $\varrho^n = \rho^n_{SE_{n+1}}$ for the joint state of SE_{n+1} at time n. The entire dynamics can then be captured by the stroboscopic, Markovian, completely positive trace preserving (CPTP) evolution

$$\varrho^{n+1} = \Phi(\varrho^n), \tag{5}$$

and the corresponding sequence of states $\varrho^0, \varrho^1, \varrho^2, \dots$ that it generates. At each step, the reduced state of the system is always available as $\rho^n_S = \mathrm{tr}_{E_{n+1}}\varrho^n$. The Markovian embedding (5) will be central to our paper. For, as we now show, all relevant properties characterizing the non-Markovianity of the evolution can be compactly computed from it. This is one of the main advantages of using collisional models to study non-Markovianity, as it allows for a clean depiction of the dynamics in terms of a single CPTP map.

Since initially the system is uncorrelated from all ancillas, it is possible to define a CPTP map taking $\rho^0_S \to \rho^n_S$:

$$\rho^n_S = \mathcal{E}_n\left(\rho^0_S\right) = \mathrm{tr}_{E_{n+1}}\Phi^n\left(\rho^0_S \otimes \rho_{E_1}\right). \tag{6}$$

But since the dynamics is non-Markovian, even though a map taking $\rho^m_S \to \rho^n_S$ may be formally defined, this map will generally not be CPTP [see Sec. (II D)].

B. Mutual information

Non-Markovianity and backflow of information must be related to correlations that develop between system and bath. However, when a system interacts with multiple modes of the bath at the same time, there are many different correlations one may consider, between the system and all possible parts of the bath. And it is not clear which of these correlations are relevant for the non-Markovian evolution. For instance, the correlation with a part of the bath with which the system will never interact again is irrelevant, as far as non-Markovianity is concerned. But in the standard scenario, it is in general not possible to identify which are the relevant correlations.

In a collisional model picture, on the other hand, this is unambiguous: the relevant correlations are those between S and ancilla E_{n+1} at time n (immediately *before* they interact). These are the correlations that ancilla E_n transferred to E_{n+1} after its interaction. Hence, they represent the only possible source of information backflow at each collision. Conveniently, this is also exactly what the Markovian embedding (5) offers. A useful measure of correlations, for instance, is the quantum mutual information (MI), defined as

$$\mathcal{I}^n(SE_{n+1}) = S\left(\rho^n_S\right) + S\left(\rho^n_{E_{n+1}}\right) - S(\varrho^n), \tag{7}$$

where $S(\rho) = -\mathrm{tr}(\rho\ln\rho)$ is the von Neumann entropy. The states ρ^n_S and $\rho^n_{E_{n+1}}$ are both computed from ϱ^n by taking the appropriate partial trace. Thus, by monitoring ϱ^n as a function of time, one has direct access to the relevant measure of correlation. Of course, $\mathcal{I}^n(SE_{n+1})$ is not the only relevant measure of correlation. Different choices, from two-point functions, to quantifiers of entanglement and quantum discord, may also be of interest. The relevant point is that any such measure will, necessarily, be contained in ϱ^n.

C. Memory kernel

In the original formulation of Nakajima [19] and Zwanzig [20], the MK was represented as a single-parameter con-

tinuous superoperator $\mathcal{K}_t$ that quantifies the memory that is retained about the system's configuration a time t in the past [see Eq. (1)]. The collisional model analog of that will be a superoperator $\mathcal{K}_n$, labeled by the discrete time index n. Thus, the stroboscopic analog of Eq. (1) should be of the form

$$\rho_S^n = \sum_{m=0}^{n-1} \mathcal{K}_{n-m}\big(\rho_S^m\big). \tag{8}$$

For instance, $\rho_S^3 = \mathcal{K}_1(\rho_S^2) + \mathcal{K}_2(\rho_S^1) + \mathcal{K}_3(\rho_S^0)$. The term $\mathcal{K}_1(\rho_S^{n-1})$ describes the short-term memory from the very last step, while $\mathcal{K}_n(\rho_S^0)$ describes the long-term memory all the way from the initial state. An explicit formula for the MK can be constructed using a reasoning similar to that used for transfer tensors in Ref. [27]: Starting with the reduced map $\mathcal{E}_n$ in Eq. (6), we define the MK recursively from

$$\mathcal{K}_n = \mathcal{E}_n - \sum_{m=1}^{n-1} \mathcal{K}_{n-m}\mathcal{E}_m. \tag{9}$$

That this is indeed the correct formula can now be verified by substituting this back in Eq. (8). For instance, $\mathcal{K}_1 = \mathcal{E}_1$, $\mathcal{K}_2 = \mathcal{E}_2 - \mathcal{K}_1\mathcal{E}_1$, $\mathcal{K}_3 = \mathcal{E}_3 - \mathcal{K}_2\mathcal{E}_1 - \mathcal{K}_1\mathcal{E}_2$, and so on. Equation (9) provides an algorithmic method for computing the MK. However, this requires heavy numerics, even in simple cases. For instance, $\mathcal{K}_3 = \mathcal{E}_3 - \mathcal{E}_2\mathcal{E}_1 - \mathcal{E}_1\mathcal{E}_2 + \mathcal{E}_1\mathcal{E}_1\mathcal{E}_1$, and the complexity of the formulas only grows from there. One of the main results in this paper will be to show that, for the case of Gaussian collisions, it is possible to write down a closed and compact formula for $\mathcal{K}_n$ (Sec. IV), which provides valuable insight into the inner workings of the memory kernel.

D. CP divisibility

The map from $\rho_S^0 \to \rho_S^n$ in Eq. (6) is always CPTP by construction. One may also define more general maps $\mathcal{E}_{m\to n}$ taking $\rho_S^m \to \rho_S^n$ $(m < n)$. Assuming that $\mathcal{E}_n^{-1}$ exists, they are defined as [4]

$$\mathcal{E}_{m\to n} = \mathcal{E}_n \circ \mathcal{E}_m^{-1}. \tag{10}$$

Albeit mathematically well defined, these maps are in general not CP. Markovian maps, on the other hand, are CP by construction. This defines the notion of CP divisibility, which provides a widely used criteria for characterizing non-Markovianity: a map is CP divisible when the intermediate maps $\mathcal{E}_{m\to n}$ are CP.

Testing CP divisibility, however, is not always easy. For instance, it may require analyzing the distance between different pairs of initial conditions ρ_S^0 [4]. According to the data processing inequality, these distances are always contractive for CP maps. Violations of contractivity are thus identified as violations of divisibility. This, however, requires a maximization over all possible initial conditions. In Sec. V we discuss the Gaussian version of this concept and show that the maximization is replaced by an alternative condition, that provides a clean and easily applicable formula for quantifying CP divisibility.

III. GAUSSIAN COLLISIONAL MODELS

The results of Sec. II are quite general, and hold for any type of system, ancillas, and interactions. However, they usually rely on heavy numerics and also lack in physical insights. In this section we specialize them to the case of continuous variables. Using the framework of Gaussian states and Gaussian-preserving operators, we show that both of the aforementioned difficulties can be overcome, leading to a transparent and insightful formulation of non-Markovianity.

A. Gaussian states and Gaussian operations

Quantifying and understanding non-Markovianity in the collisional model (3) is a task that often has to be tackled numerically. This is specially the case if one is interested in arbitrarily long times. Here we are interested in obtaining analytical results. To accomplish this, we therefore specialize now to the case of continuous-variable systems undergoing Gaussian-preserving dynamics. Our exposition, in what follows, will be example oriented. However, the final results will be general [Eqs. (23), (24), and (26)].

We assume the system is described by a bosonic annihilation operator a and corresponding quadratures $Q = (a + a^\dagger)/\sqrt{2}$ and $P = i(a^\dagger - a)/\sqrt{2}$. Similarly, the ancillas are described by bosonic annihilation operators $b_1, b_2, \ldots$, with corresponding quadratures q_n, p_n. The generalization to a multimode system, or multimode ancillas, is straightforward. We take the system-ancilla interaction U_n in Eq. (3) to be a simple beam-splitter (BS) type unitary,

$$U_n = e^{\lambda_s(a^\dagger b_n - b_n^\dagger a)}, \tag{11}$$

described by a parameter λ_s. One can view (11) as an interaction with a Hamiltonian $ig(a^\dagger b_n - b_n^\dagger a)$ that lasts for a time τ such that $g\tau = \lambda_s$. Since we are only interested in the stroboscopic dynamics, we can omit these internal details for simplicity. As for the E_nE_{n+1} collision unitary $V_{n,n+1}$, we shall explore two possibilities. The first is again a beam-splitter map

$$V_{n,n+1} = e^{\lambda_e(b_n^\dagger b_{n+1} - b_{n+1}^\dagger b_n)}, \tag{12}$$

with interaction strength λ_e. We shall henceforth refer to this as the BS dynamics. In addition, we shall also look at a two-mode squeezing (TMS) interaction,

$$\tilde{V}_{n,n+1} = e^{\nu_e(b_n^\dagger b_{n+1}^\dagger - b_{n+1} b_n)}, \tag{13}$$

with strength ν_e. The reason behind this choice is related to the fact that two-mode squeezing interactions generate stronger forms of correlations (e.g., entanglement) between the ancillas. By contrasting (12) and (13) we may therefore explore the role of quantum correlations in non-Markovianity.

The unitaries (11)–(13) are Gaussian preserving. If we assume that the initial state is Gaussian, the dynamics will then be completely characterized by the first and second moments. We assume, for simplicity, that the first moments are initially zero, so that they will remain so throughout. The covariance matrix (CM) is defined as $\sigma_{ij} = \frac{1}{2}\langle\{R_i, R_j\}\rangle$ where $\boldsymbol{R} = (Q, P, q_1, p_1, q_2, p_2, \ldots)$. The initial state is block diagonal, of the form

$$\sigma^0 = \mathrm{diag}(\theta^0, \epsilon, \epsilon, \epsilon, \ldots), \tag{14}$$

where each block is 2×2: θ^0 is the arbitrary initial CM of the system and ϵ is the initial CM of the ancillas (which are all the same, since we are assuming the ancillas are independent and identically distributed). In the analyses below we will usually take $\epsilon = \mathbb{I}_2/2$ (i.e., a vacuum state), but we leave it general for the moment.

The global dynamics of $SE_1E_2\ldots$ is unitary. As a consequence, the map (2) is translated into a symplectic evolution for the CM:

$$\sigma^n = S_{n,n+1} S_n \, \sigma^{n-1} S_n^{\mathrm{T}} S_{n,n+1}^{\mathrm{T}}, \tag{15}$$

where S_n and $S_{n,n+1}$ are the symplectic matrices associated with the unitaries U_n and $V_{n,n+1}$. The symplectic matrix associated to the beam-splitter interaction (11) is remarkably simple because all entries become proportional to the 2×2 identity [this is partially because of the choice of phase in the exponent of (11)]. For instance, the interaction S_2 between the S and E_2 reads

$$S_2 = \begin{pmatrix} x & 0 & y & 0 & \ldots \\ 0 & 1 & 0 & 0 & \ldots \\ -y & 0 & x & 0 & \ldots \\ 0 & 0 & 0 & 1 & \ldots \\ \vdots & \vdots & \vdots & \vdots & \ddots \end{pmatrix}, \tag{16}$$

where each entry is a 2×2 matrix, with $x = \cos(\lambda_s)$ and $y = \sin(\lambda_s)$. The extension to S_n is straightforward. The same structure also holds for the BS unitary $V_{n,n+1}$ between E_nE_{n+1} [Eq. (12)], except that now the position of the nonzero entries changes. For instance,

$$S_{1,2} = \begin{pmatrix} 1 & 0 & 0 & 0 & \ldots \\ 0 & z & w & 0 & \ldots \\ 0 & -w & z & 0 & \ldots \\ 0 & 0 & 0 & 1 & \ldots \\ \vdots & \vdots & \vdots & \vdots & \ddots \end{pmatrix}, \tag{17}$$

where $z = \cos(\lambda_e)$ and $w = \sin(\lambda_e)$. The TMS interaction (13) is slightly more complicated since some entries are proportional to the identity, while others are proportional to the Pauli matrix σ_z; for instance,

$$\tilde{S}_{1,2} = \begin{pmatrix} 1 & 0 & 0 & 0 & \ldots \\ 0 & \tilde{z} & \tilde{w}\sigma_z & 0 & \ldots \\ 0 & \tilde{w}\sigma_z & \tilde{z} & 0 & \ldots \\ 0 & 0 & 0 & 1 & \ldots \\ \vdots & \vdots & \vdots & \vdots & \ddots \end{pmatrix}, \tag{18}$$

with $\tilde{z} = \cosh(\nu_e)$ and $\tilde{w} = \sinh(\nu_e)$.

The BS dynamics is completely characterized by the pair (λ_s, λ_e), while the TMS dynamics is characterized by (λ_s, ν_e). On top of that, one also has the choice of ancilla initial state ϵ, which in all analyses below will be taken as the vacuum.

More general Gaussian maps will continue to have a similar structure. The symplectic S_n will have the form

$$S_2 = \begin{pmatrix} A & 0 & B & 0 & \ldots \\ 0 & 1 & 0 & 0 & \ldots \\ C & 0 & D & 0 & \ldots \\ 0 & 0 & 0 & 1 & \ldots \\ \vdots & \vdots & \vdots & \vdots & \ddots \end{pmatrix}, \tag{19}$$

for block matrices A, B, C, D. The matrices S_n for other values of n are obtained by simply placing A, B, C, D at the correct positions. Note also that the condition that S must be symplectic imposes constraints on A, B, C, D which, however, are not particularly illuminating. Similarly, the E_nE_{n+1} interaction reads

$$\tilde{S}_{1,2} = \begin{pmatrix} 1 & 0 & 0 & 0 & \ldots \\ 0 & E & F & 0 & \ldots \\ 0 & G & J & 0 & \ldots \\ 0 & 0 & 0 & 1 & \ldots \\ \vdots & \vdots & \vdots & \vdots & \ddots \end{pmatrix}, \tag{20}$$

for block matrices E, F, G, J. Note that these two expressions also naturally contemplate the case where either the system or each ancilla is, individually, composed of multiple modes (which would simply affect the size of the matrices $A, \ldots, J$).

B. Matrix difference equations for the Markovian embedding

The biggest advantage of Gaussian collisional models, as we will now show, is that the full non-Markovian evolution can be converted into a simple system of matrix difference equations for only a handful of entries of the full CM σ^n. As already discussed below Eq. (3), the step from σ^{n-1} to σ^n involves only S, E_n, and E_{n+1}. At time $n-1$ the ancilla E_{n+1} is still uncorrelated from the rest, whereas S and E_n are already correlated because of the previous step. Thus, the tripartite CM of SE_nE_{n+1}, at time $n-1$, will have the block structure

$$\sigma^{n-1}_{SE_nE_{n+1}} = \begin{pmatrix} \theta^{n-1} & \xi_n^{n-1} & 0 \\ \xi_n^{n-1,\mathrm{T}} & \epsilon_n^{n-1} & 0 \\ 0 & 0 & \epsilon \end{pmatrix}, \tag{21}$$

where ϵ_n^{n-1} is the state of ancilla E_n at time $n-1$, which is no longer the original value ϵ because it already interacted with E_{n-1} in the previous step. Moreover, ξ_n^{n-1} are the correlations between SE_n that were developed in the previous step.

We now apply the map (15) to Eq. (21), using the matrices in Eqs. (16)–(18). This will lead to a matrix σ^n with many nonzero entries. However, as far as the dynamics of S is concerned, only three entries are needed: the state of the system θ^n, the state ϵ_{n+1}^n of ancilla E_{n+1}, and the correlations ξ_{n+1}^n between S and E_{n+1}.

To gain intuition, let us first analyze the BS case, which is simple since all blocks in Eq. (17) are proportional to the identity. Using Eqs. (16) and (17) in (15), one finds the following system of matrix difference equations:

$$\begin{aligned} \theta^n &= x^2\theta^{n-1} + y^2\epsilon_n^{n-1} + xy\big(\xi_n^{n-1} + \xi_n^{n-1,\mathrm{T}}\big), \\ \epsilon_{n+1}^n &= z^2\epsilon + w^2\big[x^2\epsilon_n^{n-1} + y^2\theta^{n-1} - xy\big(\xi_n^{n-1} + \xi_n^{n-1,\mathrm{T}}\big)\big], \\ \xi_{n+1}^n &= w\big[xy\big(\theta^{n-1} - \epsilon_n^{n-1}\big) + y^2\xi_n^{n-1,\mathrm{T}} - x^2\xi_n^{n-1}\big]. \end{aligned} \tag{22}$$

This provides a neat illustration of the map $\Phi(\cdot)$ in Eq. (4): the quantities on the left-hand and right-hand side refer to different ancillas: for instance, ϵ_{n+1}^n is the state of ancilla E_{n+1} at time n, whereas ϵ_n^{n-1} is the state of E_n at time $n-1$. Of course, one could also compute ϵ_n^n, but this is not necessary for describing the dynamics of S.

The system of matrix difference equations (22) contains the minimum amount of information required to fully account

for the dynamics of S. These equations can also be recast in a more compact form in terms of the Markovian embedding (5). We define the reduced CM of SE_{n+1} at time n as

$$\gamma^n_{n+1} \equiv \gamma^n = \begin{pmatrix} \theta^n & \xi^n_{n+1} \\ \xi^{n,\mathrm{T}}_{n+1} & \epsilon^n_{n+1} \end{pmatrix}, \tag{23}$$

where the notation γ^n will be used to simplify the expressions. Equation (22) can then be written compactly as

$$\gamma^{n+1} = X\gamma^n X^{\mathrm{T}} + Y, \tag{24}$$

where the time index was shifted by 1. Here X and Y are 4×4 matrices with block form

$$X = \begin{pmatrix} x & y \\ yw & -wx \end{pmatrix}, \qquad Y = \begin{pmatrix} 0 & 0 \\ 0 & z^2\epsilon \end{pmatrix}, \tag{25}$$

where, again, each block is proportional to the identity.

Equation (24) beautifully illustrates the notion of Markovian embedding. It has the structure of a typical Gaussian CPTP map [58], being Markovian (time local) by construction. However, this Markovian dynamics takes place at the larger space of the system plus one ancilla (which one, specifically, changes at each collision). Thus, we have embedded the non-Markovian dynamics into a Markovian dynamics at a larger space. Notice how the size of the space is directly related to the fact that we chose E_n to only interact with its nearest neighbor E_{n+1}. That is, we fixed the memory length to be 1, which defines the size of the minimal space required for the embedding [54].

The matrices (25) refer to the beam-splitter unitary (12). The generalization to the arbitrary Gaussian interactions (19) and (20) is similar, albeit more cumbersome. The result is

$$X = \begin{pmatrix} A & B \\ GC & GD \end{pmatrix}, \qquad Y = \begin{pmatrix} 0 & 0 \\ 0 & J\epsilon J^{\mathrm{T}} \end{pmatrix}. \tag{26}$$

For instance, in the case of the TMS interaction, Eq. (18), one has $G = \tilde{w}\sigma_z$ and $J = \tilde{z}$, in addition to $A = D = x$, $B = y$, and $C = -y$ [which come from S_n in (16)]. One then finds that

$$X = \begin{pmatrix} x & y \\ -y\tilde{w}\sigma_z & \tilde{w}x\sigma_z \end{pmatrix}, \qquad Y = \begin{pmatrix} 0 & 0 \\ 0 & \tilde{z}^2\epsilon \end{pmatrix}. \tag{27}$$

The blocks in X are therefore no longer proportional to the identity, but some are proportional to σ_z.

To summarize, the general non-Markovian dynamics will be described by the embedding (24), with γ^n defined in (23), and with X and Y given by (26). This framework therefore provides a quite general platform, enabling one to study a broad range of situations.

C. Example dynamics

Equations (24)–(27) are the first main results of this paper. They provide a compact and efficient way of describing the non-Markovian dynamics of a bosonic mode in terms of a simple matrix difference equation for the augmented CM γ^n. The reduced state of the system is always readily accessible from the first 2×2 block [Eq. (23)]. Before proceeding to quantify the non-Markovianity of the process, we first illustrate the typical behavior of the BS and TMS maps, by plotting the average system occupation $\langle a^\dagger a\rangle$ as a function of time for different values of the E_nE_{n+1} interaction strength λ_e (for the BS case) or ν_e (for the TMS case). We choose the system to start in a thermal state with occupation number $\langle a^\dagger a\rangle^0 = 20$, while the ancillas start in the vacuum, $\epsilon = \mathbb{I}_2/2$. The results are summarized in Fig. 2, for the BS (a, b) and TMS (c, d) evolutions.

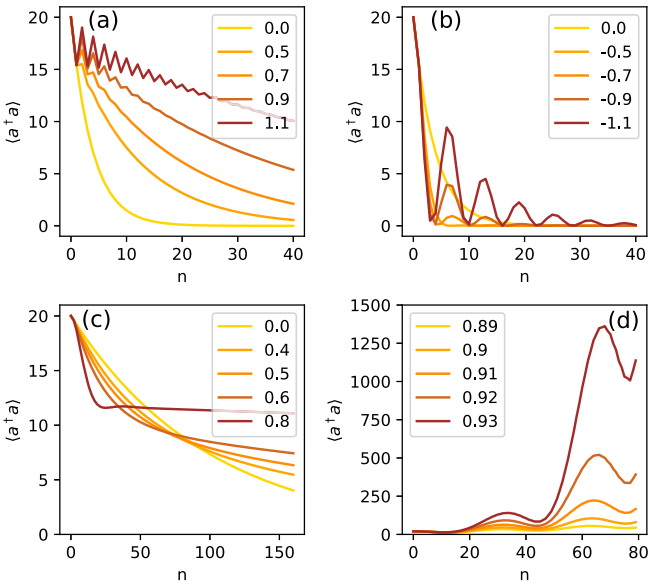

FIG. 2. Number of excitations in the system as a function of time, computed from Eq. (24). [(a),(b)] BS dynamics (25) with $\lambda_s = 0.5$ and different values of λ_e [with $\lambda_e > 0$ in (a) and $\lambda_e < 0$ in (b)]. (c, d) Same, but for the TMS dynamics (27), with $\lambda_s = 0.1$ and different values of ν_e [with $\nu_e < \nu_e^{\mathrm{crit}}$ in (a) and $\nu_e \geqslant \nu_e^{\mathrm{crit}}$ in (b), where $\nu_e^{\mathrm{crit}} = \sinh^{-1}(1) \simeq 0.8813$]. The ancillas are assumed to start in the vacuum, and the system in a thermal state with $\langle a^\dagger a\rangle^0 = 20$.

The BS dynamics is sensitive to the relative signs between λ_s and λ_e [and, consequently, of $y = \sin(\lambda_s)$ and $w = \sin(\lambda_e)$]. This is an interference effect, which occurs due to the fact we are combining two beam splitters [Eqs. (11) and (12)]. A similar effect was also observed in Refs. [56,57]. We emphasize this in Figs. 2(a) and 2(b) by comparing $\lambda_e > 0$ and $\lambda_e < 0$, with $\lambda_s > 0$. In both cases we see that for small λ_e the excitations tend to decay monotonically, which is what one would expect of a Markovian BS interaction with a vacuum bath. For larger λ_e, on the other hand, the occupations present oscillations. Since the interaction conserves the number of quanta, these revivals in excitations must necessarily be due to a backflow caused by the non-Markovian behavior. That is, some of the excitations that leave the system towards E_n are transferred from E_n to E_{n+1} and then make it back into the system in the SE_{n+1} interaction. The nature of these oscillations, however, is different whether $\lambda_e > 0$ or $\lambda_e < 0$, being fast in the former and slow in the latter. Irrespective of the value of λ_e, however, after an infinite time the system will always thermalize to the ancilla's state, which in this case means $\langle a^\dagger a\rangle^\infty = 0$ [the only exception is at $\lambda_e = \pm\pi/2$, which is somewhat pathological].

Results for the TMS interaction are shown in Figs. 2(c) and 2(d). In this case the relative signs are immaterial, but the dynamics becomes more sensitive to the magnitude of ν_e, since $\tilde{z}$ and $\tilde{w}$ are hyperbolic functions. The TMS interaction entangles E_nE_{n+1}, even if both are initially in the vacuum. As

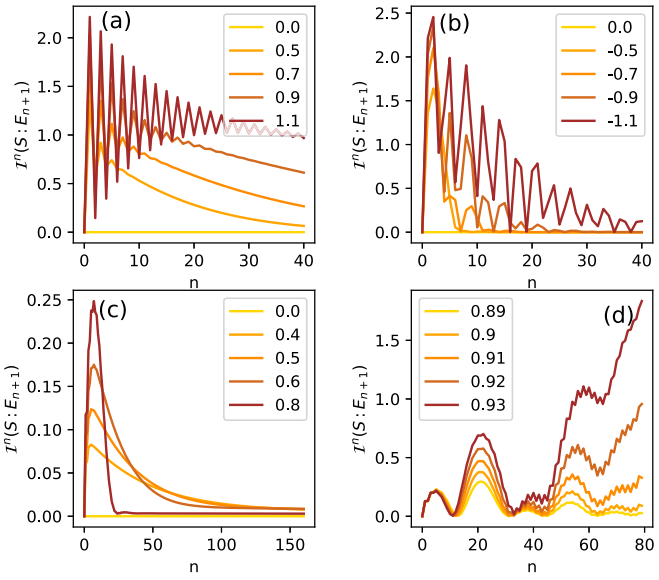

FIG. 3. Mutual Information (7) for the BS (a, b) and TMS (c, d) dynamics. Other parameters are the same as Fig. 2.

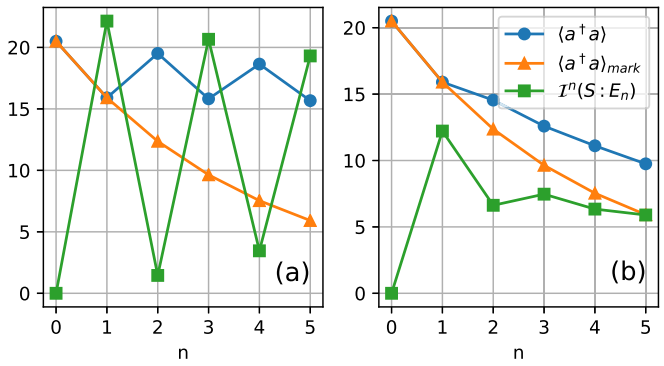

FIG. 4. Comparison between Markovian and non-Markovian dynamics and role of the mutual information. In blue circles we show the early dynamics of $\langle a^\dagger a\rangle$ vs n for the BS dynamics with (a) $\lambda_e = 1.1$ and (b) $\lambda_e = 0.3$, with fixed $\lambda_s = 0.5$ [see Fig. 2(a)]. The corresponding Markovian case ($\lambda_e = 0$) is shown in orange triangles. These curves are to be compared with the MI (7), shown by green squares in the two cases [Fig. 3(a)]. The heights of each curve were adjusted for better visibility.

a consequence, it also spontaneously creates excitations, so that the number of quanta is not preserved. At each E_nE_{n+1} collision the net number of excitations therefore increases. Some of these excitations are lost when the ancillas are discarded and some flow to the system. As a consequence, depending on the rate at which excitations are created, the dynamics can be either stable or unstable. This occurs at the critical point $\nu_e^{\rm crit} = \sinh^{-1}(1) \simeq 0.8813$, which is when $\tilde{w} = 1$, thus marking the situation where the number of excitations in the system grow unboundedly [see Eq. (27)]. When $\nu_e < \nu_e^{\rm crit}$ the dynamics will be stable and the system will converge to a steady-state value $\langle a^\dagger a\rangle = \sinh^2 \nu_e (1 - \sinh^2 \nu_e)^{-1}$ independently of λ_s [Fig. 2(c)]. Conversely, for $\nu_e \geqslant \nu_e^{\rm crit}$, the dynamics becomes unstable and the number of excitations diverges [Fig. 2(d)]. These asymptotic values can be understood from arguments of stability theory, as shown in Appendix A.

D. Mutual information

The Gaussian framework used here makes the MI (7) readily accessible from the CM γ^n in Eq. (23). Correlations are related to the off-diagonal blocks ξ^n_{n+1} (the MI would be zero if γ^n was block diagonal). The three entropies in Eq. (7) can be readily computed in terms of the symplectic eigenvalues of γ^n [58]. The results are shown in Fig. 3, for the same collection of parameters as Fig. 2 As a sanity check, the MI is identically zero when $\lambda_e = \nu_e = 0$. It also tends to be larger for short times, tending to zero as n grows. The only exception is the unstable dynamics in Fig. 3(d), where the MI grows unboundedly. The oscillatory patterns in $\langle a^\dagger a\rangle$ are also present in the MI.

To better understand the role of the MI in the non-Markovian dynamics we present in Fig. 4 a comparison between the occupation number $\langle a^\dagger a\rangle$ of Fig. 2 and the MI of Fig. 3 for the BS dynamics. We focus on early times (small n) and also compare $\langle a^\dagger a\rangle$ with the corresponding Markovian dynamics ($\lambda_e = 0$). The difference between the non-Markovian (blue circles) and Markovian (orange triangles) dynamics reflects the extent to which the backflow of information affects the evolution. This, as can be seen in the figure, is directly correlated with the MI (green squares) *of the previous step*. That is, a large MI in a given step implies a large difference between the blue and orange curves in the following one. This is particularly clear in Fig. 4(a) and serves to illustrate how the correlations built between SE_{n+1}, at step n, affect the future interaction between S and E_{n+1} at the next step.

IV. MEMORY KERNEL

The MK discussed in Eqs. (1) and (8), and Sec. II C, is perhaps the most physically transparent way of analyzing non-Markovianity [see also Fig. 1(c)]. Starting from any global map between system and bath, one can always write down a differential equation for the reduced density matrix ρ_S of the system. This equation, however, will in general be time-nonlocal; i.e., it will be an integrodifferential equation of the form (1), where $\mathcal{K}_{t-t'}[\rho_S(t')]$ describes how $d\rho_S(t)/dt$ depends on $\rho_S(t')$ in previous times $t' < t$. The MK therefore contains all the information about the dynamics, with non-Markovianity being related to its overall dependence on $t - t'$: the slower the decay of $\mathcal{K}_{t-t'}$ with $t - t'$, the longer the memory and hence the more non-Markovian is the dynamics. The Markovian case is recovered when $\mathcal{K}_{t-t'} \propto \delta(t - t')$.

The memory kernel $\mathcal{K}_{t-t'}$ is a superoperator acting on the full Hilbert space of the system. Computing it is thus, in general, a very difficult task. Within our framework, however, one may equivalently formulate a memory kernel acting only in the system's CM θ^n. This can be accomplished starting from Eq. (24) and writing down a difference equation for θ^n only. As we will demonstrate below, this equation will have the form [contrast with (8)]

$$\theta^{n+1} = x^2\theta^n + \sum_{r=0}^{n-1} \mathcal{K}_{n-r-1}(\theta^r) + G_n, \tag{28}$$

where G_n is a contribution that depends only on the initial state of the ancillas [68] and $\mathcal{K}_n$ is the memory kernel. The way we define it, the MK is such that $\mathcal{K}_0$ measures how the step from θ^n to θ^{n+1} is affected by θ^{n-1} and $\mathcal{K}_{n-1}$ measures how it is affected by θ^0. $\mathcal{K}_n$ is still a superoperator, but one which acts on the space of 2×2 CMs. One can write it more explicitly in terms of a Kraus operator-sum representation [69,70]

$$\mathcal{K}_n(\theta) = \sum_{ij} \kappa_{ij}^n M_i \theta M_j^{\mathrm{T}}, \tag{29}$$

where κ_{ij}^n are coefficients that depend on time and $\{M_i\}$ is a complete set of 2×2 matrices; a convenient choice is the set of Pauli matrices $\{\mathbb{I}_2, \sigma_z, \sigma_+, \sigma_-\}$. A general recipe to compute the coefficients κ_{ij}^n in Eq. (29) is given below in Eq. (48). Crucially, as we show, it depends *only* on the matrix X of the Markovian embedding (24).

The memory itself is contained in the dependence of κ_{ij}^n on n. The dependence on i, j determines how different elements of θ^r affect θ^n. For instance, as we will show below, in the case of the BS map [Eq. (25)], the only nonzero coefficient will be the one proportional to $\mathbb{I}_2 \theta \mathbb{I}_2 = \theta$, which we refer to as κ_{11}^n; that is, the memory kernel is actually a c number, $\mathcal{K}_n(\theta) = \kappa_{11}^n \theta$. This implies that the MK is the same for all entries of θ^n and each entry $(\theta^n)_{ij}$ is only affected by the corresponding entry $(\theta^r)_{ij}$ at past times. Conversely, in the TMS map there will be four nonzero coefficients, corresponding to combinations of $M_1 = \mathbb{I}_2$ and $M_2 = \sigma_z$; we refer to them as κ_{11}^n, $\kappa_{1,z}^n$, $\kappa_{z,1}^n$, and $\kappa_{z,z}^n$. This means that the memory kernel of $(\theta^n)_{11}$ will be different from that of $(\theta^n)_{2,2}$ and so on (each entry will have its own memory kernel). Finally, a memory kernel containing a dependence on $\sigma_\pm$ would imply that $(\theta^n)_{11}$ would depend on the past values of other entries, such as $(\theta^r)_{12}$ and $(\theta^r)_{22}$.

A. General derivation of the memory kernel

We now carry out the derivation of the memory kernel and transfer tensor for the Gaussian collisional model. Since we are unaware of any other papers doing this, we consider here a more general scenario, which relies only on the structure of the Markovian embedding in Eq. (24). We also assume that the system and ancillas are each composed of an arbitrary number of modes N_S and N_E [Eqs. (25) and (27) are recovered for $N_S = N_E = 1$]. More specifically, we take the matrices X and Y to have the following block structure:

$$X = \begin{pmatrix} X_{11} & X_{12} \\ X_{21} & X_{22} \end{pmatrix}, \qquad Y = \begin{pmatrix} 0 & 0 \\ 0 & Y_{22} \end{pmatrix}, \tag{30}$$

where, e.g., X_{11} and X_{22} are of size $2N_S$ and $2N_E$, respectively. This therefore contemplates both multimode system and ancillas, as well as collisions with longer memory. For instance, if E_n collides with E_{n+1} and E_{n+2}, then we would have $N_S = 1$ and $N_E = 2$.

Our derivation follows the general approach of Nakajima [19] and Zwanzig [20], but adapted to the present context. We begin by noting the following property: The solution of a generic difference equation of the form

$$\psi(n+1) = \alpha \psi(n) + g(n) \tag{31}$$

is given by

$$\psi(n) = \alpha^n \psi(0)_+ \sum_{r=0}^{n-1} \alpha^{n-r-1} g(r). \tag{32}$$

This solution holds for arbitrary objects ψ, provided α is a linear operator. It therefore holds when ψ is a vector and α is a matrix, or when ψ is a matrix and α is a superoperator. Thus, for instance, the solution of Eq. (24) is

$$\gamma^n = X^n \gamma^0 (X^{\mathrm{T}})^n + \sum_{r=0}^{n-1} X^{n-r-1} Y (X^{\mathrm{T}})^{n-r-1}. \tag{33}$$

Here the notation γ^n, to denote the time index, becomes a bit ambiguous since X^n is the matrix X to the power n. But there is no room for confusion, since X^n will be the only quantity where the superscript does not refer to the time.

We now introduce the vectorization operation [71], which transforms a matrix A into a vector $\vec{A} = \mathrm{vec}(A)$ by stacking its columns. For instance,

$$\mathrm{vec}\begin{pmatrix} a & b \\ c & d \end{pmatrix} = \begin{pmatrix} a \\ c \\ b \\ d \end{pmatrix}. \tag{34}$$

One may verify that, for any three matrices A, B, C,

$$\mathrm{vec}(ABC) = (C^{\mathrm{T}} \otimes A)\mathrm{vec}(B). \tag{35}$$

With this, the matrix difference equation (24) is converted into a vector difference equation

$$\vec{\gamma}^{\,n+1} = (X \otimes X)\vec{\gamma}^{\,n} + \vec{Y}. \tag{36}$$

We also introduce projection matrices onto the subspaces of system and ancilla,

$$P_S = \begin{pmatrix} \mathbb{I}_{2N_S} & 0 \\ 0 & 0 \end{pmatrix}, \qquad P_E = \begin{pmatrix} 0 & 0 \\ 0 & \mathbb{I}_{2N_E} \end{pmatrix}, \tag{37}$$

which are of size $2N_S + 2N_E$. In the larger space relevant for vectorization there are four possible projections, $P_S(\ldots)P_S$, $P_S(\ldots)P_E$, and so on. These operations chop the covariance matrix γ^n in four blocks, as in Eq. (23). Our interest is in $P_S(\gamma^n)P_S$, as it contains the system CM θ^n. We therefore also introduce

$$P = P_S \otimes P_S, \tag{38}$$

together with its complement $Q = 1 - P$. Note, though, that $Q \neq P_E \otimes P_E$.

We now multiply Eq. (36) by P and use that $P + Q = 1$, together with the fact that $P\vec{Y} = 0$ [see Eq. (30)]. We then get

$$P\vec{\gamma}^{\,n+1} = P(X \otimes X)P\vec{\gamma}^{\,n} + P(X \otimes X)Q\vec{\gamma}^{\,n}. \tag{39}$$

Similarly, multiplying Eq. (36) by Q we find

$$Q\vec{\gamma}^{\,n+1} = Q(X \otimes X)Q\vec{\gamma}^{\,n} + Q(X \otimes X)P\vec{\gamma}^{\,n} + \vec{Y}. \tag{40}$$

Now comes the crucial idea of the Nakajima [19] and Zwanzig [20] method. We interpret Eqs. (39) and (40) as two coupled equations for the variables $P\vec{\gamma}^{\,n}$ and $Q\vec{\gamma}^{\,n}$. Since our interest is in $P\vec{\gamma}^{\,n}$, we first solve Eq. (40), assuming a given $P\vec{\gamma}^{\,n}$, and then substitute the result in Eq. (39). Equation (40) is of the

form (31) with $\alpha = Q(X \otimes X)$ and $g(n) = Q(X \otimes X)P\vec{\gamma}^{\,n} + \vec{Y}$. Equation (32) then gives

$$Q\vec{\gamma}^{\,n} = [Q(X \otimes X)]^n Q\vec{\gamma}^{\,0} + \sum_{r=0}^{n-1} [Q(X \otimes X)]^{n-r-1}[Q(X \otimes X)P\vec{\gamma}^{\,r} + \vec{Y}].$$

Plugging this in Eq. (39) we then arrive at

$$P\vec{\gamma}^{\,n+1} = P(X \otimes X)P\vec{\gamma}^{\,n} + \sum_{r=0}^{n-1} \hat{K}_{n-r-1} P\vec{\gamma}^{\,r} + \vec{\mathcal{G}}_n, \tag{41}$$

where

$$\hat{K}_{n-r-1} = P(X \otimes X)[Q(X \otimes X)]^{n-r-1} Q(X \otimes X) \tag{42}$$

is the memory kernel in vectorized form [i.e., as a matrix of size $(2N_S + 2N_E)^2$]. The term $\vec{\mathcal{G}}_n$, on the other hand, is a function that depends only on the initial state of the ancillas and reads

$$\mathcal{G}_n = P(X \otimes X)[Q(X \otimes X)]^n Q\vec{\gamma}^{\,0} + \sum_{r=0}^{n-1} P(X \otimes X)[Q(X \otimes X)]^{n-r-1}\vec{Y}.$$

What is left is to rewrite Eq. (41) as an equation for the evolution of the system's CM θ^n only. We introduce the $(2N_S)^2 \times (2N_S + 2N_E)^2$ rectangular matrix π defined such that $\pi\vec{\gamma}^{\,n} = \vec{\theta}^{\,n}$. For instance, in the case $N_S = N_E = 1$, the matrix π will be 4×16, of the form (for more intuition on this matrix, see Appendix B)

$$\pi = \begin{pmatrix} 1 & 0 & 0 & 0 & 0 & 0 & 0 & 0 & \dots & 0 \\ 0 & 1 & 0 & 0 & 0 & 0 & 0 & 0 & \dots & 0 \\ 0 & 0 & 0 & 0 & 1 & 0 & 0 & 0 & \dots & 0 \\ 0 & 0 & 0 & 0 & 0 & 1 & 0 & 0 & \dots & 0 \end{pmatrix}. \tag{43}$$

We also notice that $P = \pi^{\mathrm{T}}\pi$ and $\pi\pi^{\mathrm{T}} = \mathbb{I}_{(2N_S)^2}$. Multiplying Eq. (41) on the left by π we then get

$$\vec{\theta}^{\,n+1} = (X_{11} \otimes X_{11})\vec{\theta}^{\,n} + \sum_{r=0}^{n-1} \hat{\mathcal{K}}_{n-r-1}\vec{\theta}^{\,r} + \vec{G}_n, \tag{44}$$

where we also used the fact that $\pi(X \otimes X)\pi^{\mathrm{T}} = X_{11} \otimes X_{11}$. Here $\vec{G}_n = \pi\vec{\mathcal{G}}_n$ is again a term that depends only on the initial conditions of the ancillas, whereas

$$\hat{\mathcal{K}}_n = \pi\hat{K}_n\pi^{\mathrm{T}} = \pi(X \otimes X)[Q(X \otimes X)]^{n+1}\pi^{\mathrm{T}}$$

is the memory kernel, now expressed as a matrix of size $(2N_S)^2 \times (2N_S)^2$ acting on $\vec{\theta}^{\,r}$. This can also be written more symmetrically, by exploiting the fact that $Q^2 = Q$. We can then arrange it as

$$\hat{\mathcal{K}}_n = \pi(X \otimes X)Q[Q(X \otimes X)Q]^n Q(X \otimes X)\pi^{\mathrm{T}}. \tag{45}$$

The extra Q's outside the square brackets are placed simply to ensure the result also holds for $n = 0$. This is the final form of the MK. Crucially, notice how it depends *only* on the matrix X of the Markovian embedding (24).

To obtain a matrix difference equation for θ^n we must "unvec" Eq. (44); that is, apply the inverse map of (34). Unvecking the first term is trivial since, by Eq. (35),

$$\mathrm{unvec}[(X_{11} \otimes X_{11})\vec{\theta}^{\,n}] = X_{11}\theta^n X_{11}^{\mathrm{T}}.$$

The memory kernel (45), on the other hand, cannot be unvecked as a single product of $A\theta^n B$. Instead, it is convenient to express it as

$$\hat{\mathcal{K}}_n = \sum_{ij} \kappa_{ij}^n M_j \otimes M_i, \tag{46}$$

where κ_{ij}^n are real coefficients and $\{M_i\}$ is a set of operators spanning the vector space of $2N_S$-dimensional real matrices. Decomposed in this form, the unvecked version of the memory kernel will then be, from (35),

$$\mathcal{K}_n(\theta) = \sum_{ij} \kappa_{ij}^n M_i \theta M_j^{\mathrm{T}}. \tag{47}$$

Finally, the form of the coefficients κ_{ij}^n can be found if we assume that the M_i form an orthogonal basis with respect to the Hilbert-Schmidt norm $(A|B) = \mathrm{tr}(A^{\mathrm{T}}B)$ (which is the case of the Pauli basis, for instance). Multiplying Eq. (46) by $M_j \otimes M_i$ and tracing then yields, by orthogonality,

$$\kappa_{ij}^n = \frac{\mathrm{tr}\big[(M_j^{\mathrm{T}} \otimes M_i^{\mathrm{T}})\hat{\mathcal{K}}_n\big]}{\mathrm{tr}\big(M_i^{\mathrm{T}}M_i\big)\mathrm{tr}\big(M_j^{\mathrm{T}}M_j\big)}. \tag{48}$$

This, together with Eq. (45), is all that is required to compute the memory kernel. With all these definitions, one may now finally unvec Eq. (44), leading to

$$\theta^{n+1} = X_{11}\theta^n X_{11}^{\mathrm{T}} + \sum_{r=0}^{n-1} \mathcal{K}_{n-r-1}(\theta^r) + G_n, \tag{49}$$

where $G_n = \mathrm{unvec}(\vec{G}_n) = \mathrm{unvec}(\pi\vec{\mathcal{G}}_n)$ is, again, a term depending only on the initial states of the ancillas.

B. Memory kernel for the BS dynamics

We now illustrate the memory kernel for the two maps considered in Sec. II, starting with the BS dynamics. In general, the structure of the memory kernel will be quite complicated. For the BS dynamics [Eq. (25)], however, the only nonzero coefficient in Eq. (48) is κ_{11}^n, the term proportional to the identity. In this case the memory kernel is therefore rather simple, as it is just a c number multiplying all entries of θ^r. A more compact formula for the MK in this case is given in Appendix B.

Results for the BS dynamics are shown in Fig. 5. The upper panel corresponds to $\lambda_s = 0.5$, which is similar to Eq. (2). As can be seen, for $\lambda_e > 0$ [Fig. 5(a)] the memory kernel's decay is oscillatory, with an exponential envelope. For $\lambda_e < 0$, oscillations are also observed, but these are rather different in nature and more asymmetrical with respect to the horizontal axis. When $\lambda_s = 0.05$ the situation changes [Figs. 5(c) and 5(d)]. The dynamics of $\langle a^\dagger a\rangle$ is still quite similar to that of $\lambda_s = 0.5$, shown in Fig. 2, except that the timescales become much longer. But in the MK one sees something entirely different. In particular, one finds that while κ_{11}^n continues to oscillate when $\lambda_e > 0$, it now becomes exclusively negative for $\lambda_e < 0$. In this case therefore, all past values of θ^r tend to contribute negatively to the evolution.

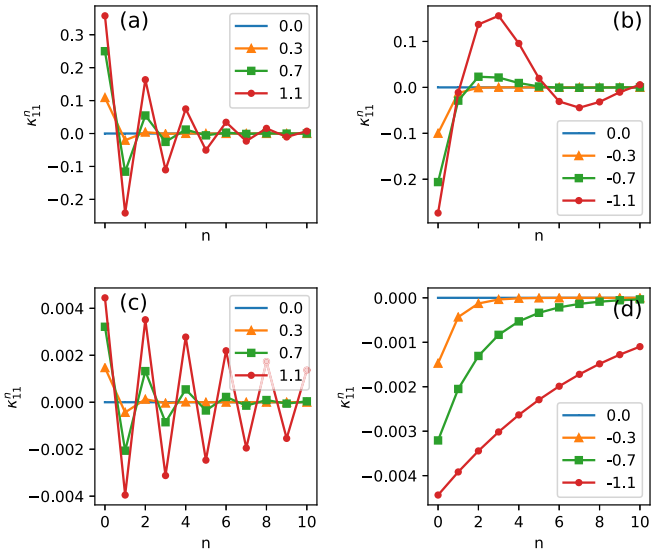

FIG. 5. The memory kernel for the BS dynamics, Eq. (25). In this case the only nonzero entry in Eq. (29) is κ^n_{11}, the term proportional to the identity. The plots are for $\lambda_s = 0.5$ (upper panel) and $\lambda_s = 0.05$ (lower panel), with $\lambda_e > 0$ (left) and $\lambda_e < 0$ (right).

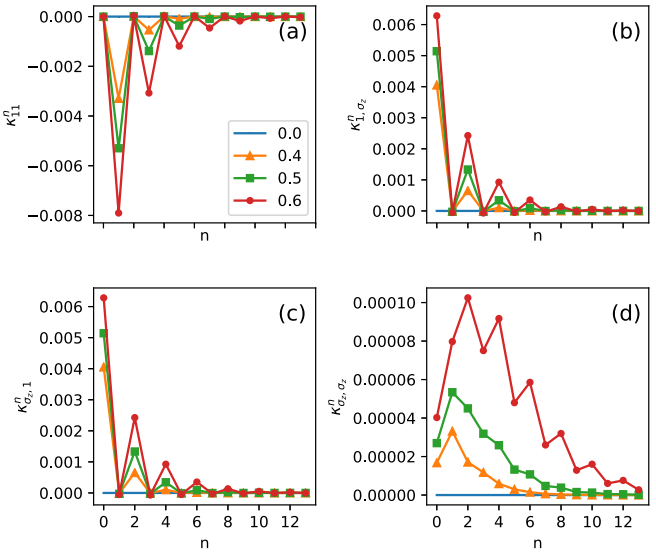

FIG. 7. The memory kernel for the (stable) TMS dynamics, Eq. (27), with $\lambda_s = 0.1$ and different values of λ_e. Each curve corresponds to a different entry of Eq. (29), namely, κ^n_{11}, κ^n_{1,σ_z}, $\kappa^n_{\sigma_z,1}$, and $\kappa^n_{\sigma_z,\sigma_z}$.

Negative values in the memory kernel are rather important, as they are associated with faster convergence. The reason is that the CM is a positive matrix and the first term in (29) is always positive. The negativities observed in Fig. 5 therefore represent an accelerated draining of excitations from the system. This sheds light on some of the behaviors previously observed for the number operator (Fig. 2) and mutual information (Fig. 3).

It is possible to condense a lot of information about the memory kernel by plotting κ^n_{11} in the (λ_s, λ_e) plane, for different values of n. This is shown in Fig. 6. Each plot corresponds to a different value of n, from 0 up to 9. The dependence on the relative signs of λ_s and λ_e is clearly visible, as is the overall damping of the memory with increasing n. Particularly interesting, this map is able to very clearly pinpoint the regions that have negative memory kernels, something which is found to be highly nontrivial.

C. Memory kernel for the TMS dynamics

Next we turn to the TMS case. In this case it is found that there are, in total,

$$\mathcal{K}_n(\theta) = \kappa^n_{11}\theta + \kappa^n_{1z}\theta\sigma_z + \kappa^n_{z1}\sigma_z\theta + \kappa^n_{zz}\sigma_z\theta\sigma_z. \tag{50}$$

These quantities are plotted in Fig. 7 for the stable dynamics ($\nu_e < \nu_e^{\text{crit}}$), with $\lambda_s = 0.1$. All four coefficients are found to decay in time in an oscillatory fashion.

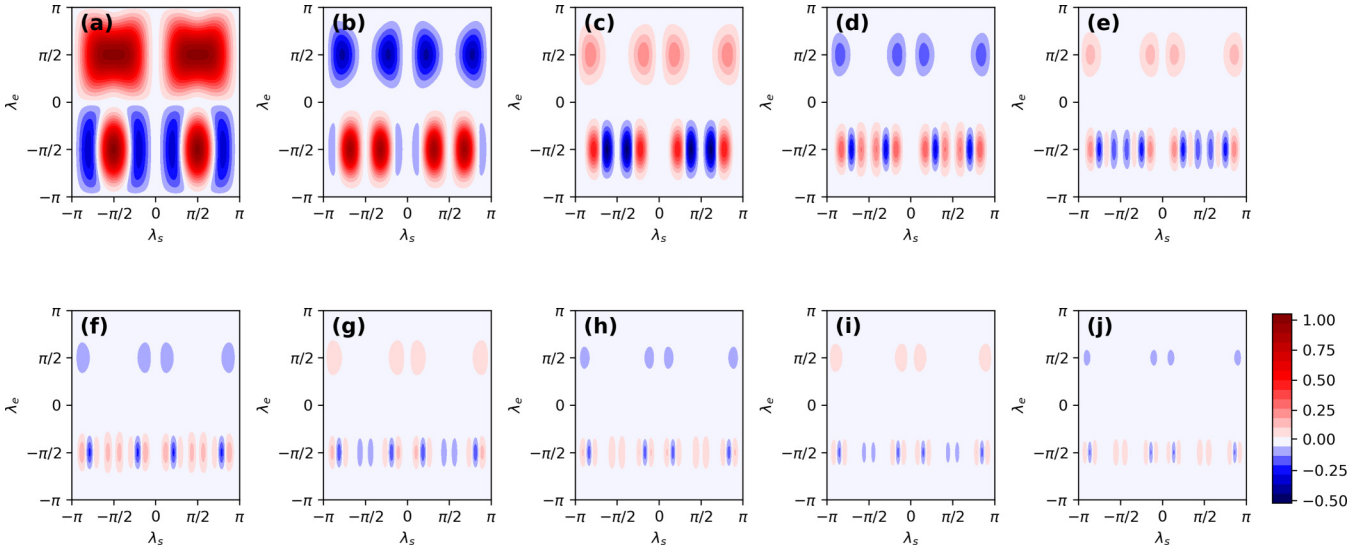

FIG. 6. Diagrams for the memory kernel of the BS dynamics. Each plot shows κ^n_{11} in the (λ_s, λ_e) plane for a different value of n, from $n = 0$ to 9.

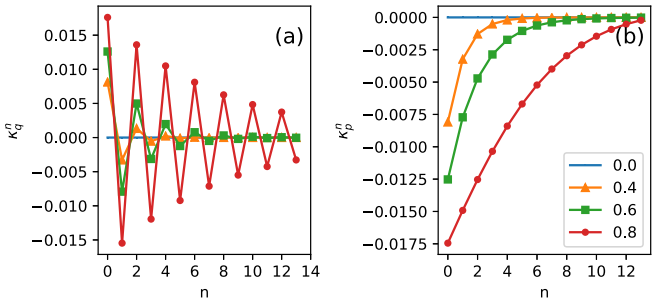

FIG. 8. The MK for $\langle Q^2\rangle$ and $\langle P^2\rangle$, Eq. (51), for the TMS dynamics. Other parameters are the same as Fig. 7.

The physics of each coefficient, however, is not necessarily transparent. In order to gain better intuition, let us focus on the diagonal entries of θ^n. In this case one finds that

$$(\mathcal{K}_n(\theta))_{11} = \left(\kappa_{11}^n + \kappa_{1z}^n + \kappa_{z1}^n + \kappa_{zz}^n\right)\theta_{11}^n := \kappa_q^n \theta_{11}^n,$$
$$(\mathcal{K}_n(\theta))_{22} = \left(\kappa_{11}^n - \kappa_{1z}^n - \kappa_{z1}^n + \kappa_{zz}^n\right)\theta_{22}^n := \kappa_p^n \theta_{22}^n. \quad (51)$$

The coefficients κ_q^n and κ_p^n therefore describe the individual memory kernels of $\langle Q^2\rangle$ and $\langle P^2\rangle$, which are different in the TMS dynamics.

These two contributions are shown in Fig. 8, for the same parameters as in Fig. 7. We also present diagrams in the (λ_s, ν_e) plane in Figs. 9 and 10. The plots in Fig. 8 reveal an extremely interesting asymmetry between the two quadratures. We see that the memory associated with $\langle Q^2\rangle$ is oscillatory, whereas that associated with $\langle P^2\rangle$ is always negative and decays monotonically. This asymmetry is a consequence of our choice of two-mode squeezing in the TMS interaction (13). Figures 9 and 10, however, show that the situation is more intricate. Indeed, for fixed (λ_s, ν_e), κ_q is found to oscillate with n. But for κ_p this is not necessarily the case.

Finally, in Fig. 11 we compare the previous result with the case of ν_e in the vicinity of, and larger than, $\nu_e^{\text{crit}} = 0.8813$, i.e., in the situation where the dynamics diverges. As can be seen, in this case both κ_q and κ_p diverge as well (notice the different scale of the horizontal axis). This is therefore contrary to our usual notion of memory: It means that the system retains a stronger memory from events in the distant past than those in the recent one. Or, to put it differently, the relative importance of past events accumulates.

V. GAUSSIAN CP DIVISIBILITY

Even though the MK explicitly shows the dependence on previous states, this alone does not necessarily imply a non-Markovian dynamic [24]. It is therefore important to contrast the MK with an actual test of non-Markovianity. Here we focus on CP divisibility of intermediate maps, introduced in Sec. II D: the formulation for Gaussian dynamics, at the level of the covariance matrix, in Refs. [72,73]. Any Gaussian CPTP map must have the form

$$\theta \to \mathcal{X}\theta\mathcal{X}^{\mathrm{T}} + \mathcal{Y},$$

where $\mathcal{X}$ and $\mathcal{Y}$ are matrices satisfying [58,74]

$$\mathcal{M}[\mathcal{X}, \mathcal{Y}] := 2\mathcal{Y} + i\Omega - i\mathcal{X}\Omega\mathcal{X}^{\mathrm{T}} \geqslant 0, \quad (52)$$

with $\Omega = i\sigma_y$ the symplectic form. Here $\mathcal{M} \geqslant 0$ means the matrix must be positive semidefinite.

In our case, the evolution of the system's CM, from time zero to n, must therefore also be of this form:

$$\theta^n = \mathcal{X}_n \theta^0 \mathcal{X}_n^{\mathrm{T}} + \mathcal{Y}_n. \quad (53)$$

The matrices $\mathcal{X}_n$ and $\mathcal{Y}_n$ can be read from the (1,1) block of the general solution (33) and are independent of the initial state θ^0, viz.,

$$\mathcal{X}_n = (X^n)_{11}, \quad (54)$$

$$\mathcal{Y}_n = (X^n)_{12}\epsilon(X^{n\mathrm{T}})_{12} + \sum_{r=0}^{n-1}[X^{n-r-1}Y(X^{\mathrm{T}})^{n-r-1}]_{11}, \quad (55)$$

where the subscripts i, j refer here to specific blocks. This easiness in reading of the corresponding map matrices is another significant advantage of the Markovian embedding representation (24).

To probe whether the dynamics is divisible, we consider the map taking the system from n to $m > n$. Assuming that $\mathcal{X}_n$ and $\mathcal{Y}_n$ are invertible, which is true in our case, this will have the form [72]

$$\theta^m = \mathcal{X}_{mn}\theta^n\mathcal{X}_{mn}^{\mathrm{T}} + \mathcal{Y}_{mn}, \quad (56)$$

where

$$\mathcal{X}_{mn} = \mathcal{X}_m\mathcal{X}_n^{-1}, \quad \mathcal{Y}_{mn} = \mathcal{Y}_m - \mathcal{X}_{mn}\mathcal{Y}_n\mathcal{X}_{mn}^{\mathrm{T}}. \quad (57)$$

See Fig. 1(d). The dynamics is then considered divisible when the intermediate maps (56) are a proper CPTP Gaussian map, that is, when $\mathcal{M}[\mathcal{X}_{mn}, \mathcal{Y}_{mn}] \geqslant 0$ [Eq. (52)].

The above criteria can be used not only as a dichotomic measure of divisibility, but also as a figure of merit [72]. This

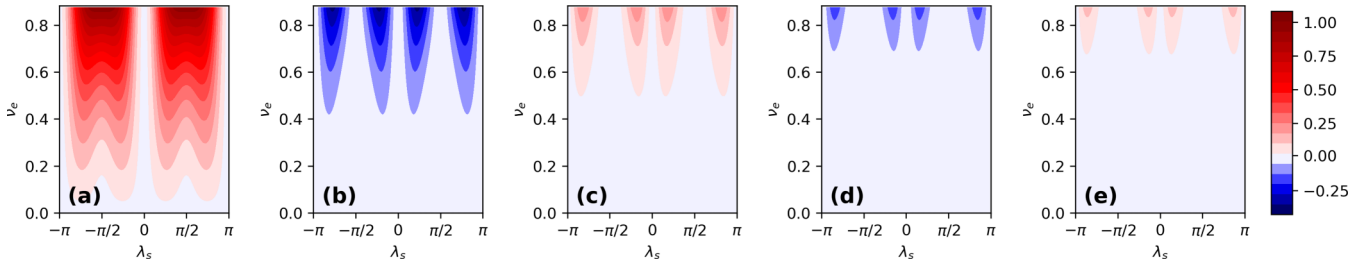

FIG. 9. Diagrams for the memory kernel coefficient κ_q^n [Eq. (51)] of the TMS dynamics, in the (λ_s, ν_e) place, for $n = 0, \ldots, 4$.

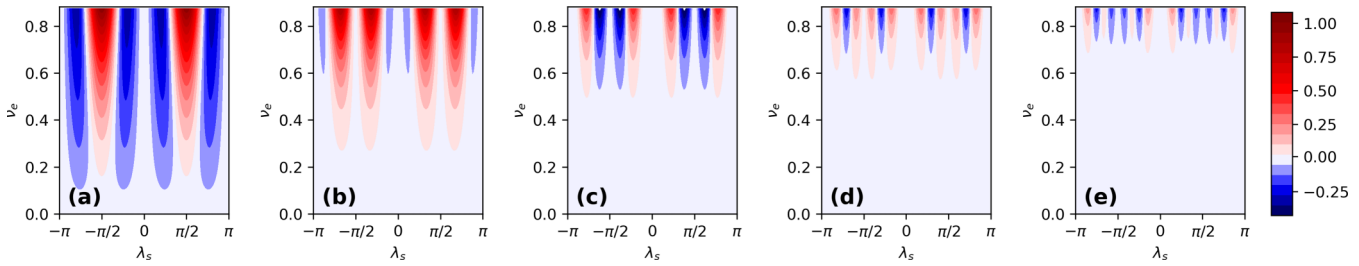

FIG. 10. Similar to Fig. 9, but for κ_p^n.

is accomplished by defining

$$\mathcal{N}_{mn} = \sum_k \frac{|m_k| - m_k}{2}, \quad \{m_k\} = \text{eigs}(\mathcal{M}[\mathcal{X}_{mn}, \mathcal{Y}_{mn}]). \tag{58}$$

This quantity is always non-negative and the map is divisible if and only if $\mathcal{N}_{mn} \equiv 0$ for all m, n. Otherwise, the magnitude of $\mathcal{N}_{mn}$ quantifies the extent to which divisibility is broken for that choice of m, n.

A. BS dynamics

We begin our investigation of $\mathcal{N}_{mn}$ by focusing on the BS dynamics [Eq. (25)]. An example of the behavior of (58) is shown in Fig. 12, where we plot $\mathcal{N}_{mn}$ in the (n, m) plane, with fixed $\lambda_s = 1.1$ and different values of λ_e. The magnitude of $\mathcal{N}_{mn}$ is represented by the size of each point. These diagrams are interpreted as follows. We start with Fig. 12(a). In this case we see that, for $n = 1$, $\mathcal{N}_{mn}$ is nonzero only for $m = 2$ and 4, being smaller in the latter. For $n = 3$ the map is always divisible. And for $n = 3$, it is not divisible only for $m = 4$ and 6. These irregularities are a consequence of the oscillatory character of the parameters appearing, e.g., in Eq. (25). Still concerning Fig. 12(a), we see notwithstanding that as n gets large, the map tends to be Markovian for all m. As we increase λ_e, however, as in Figs. 12(b) and 12(c), we see that overall the regions where $\mathcal{N}_{mn} > 0$ tend to increase. They increase both as a function of n as well as a function of m for fixed n.

When $\lambda_e < 0$, however, strange things happen [Fig. 12(d)]. In this case we find that there can be highly irregular values of (n, m) which yield nonzero $\mathcal{N}_{mn}$ which, in fact, can reach significantly large values. For instance, the largest value plotted in Fig. 12(d) is for $n = 13$, $m = 14$ and has the value $\mathcal{N} \sim 69.7$. For $n = 16$, $m = 17$, however, one finds $\mathcal{N} \sim 10\,309$ (not shown). This is to be contrasted with Fig. 12(a), the largest value of which is $\mathcal{N} = 3.42$. We present these results simply to emphasize that $\mathcal{N}_{mn}$ can oscillate violently. The reason is due to the term $\mathcal{X}_n^{-1}$ in Eq. (57), which can blow up for certain values of λ_s, λ_e, and n.

Next we turn to the divisibility of a single collision, that is, with $m = n + 1$. Plots of $\mathcal{N}_{n+1,n}$ in the (λ_s, λ_e) plane are shown in Fig. 13. The overall behavior is found to alternate with even and odd n. For n even, the map is always divisible for $\lambda_e > 0$ and potentially nondivisible within certain regions of $\lambda_e < 0$. Conversely, for n odd, one finds that divisibility breaks down in significant portions of the (λ_s, λ_e) plane. An additional illustration of the complex dependence of $\mathcal{N}_{n+1,n}$ on λ_s, λ_e, n is provided in Fig. 14, where we plot $\mathcal{N}_{n+1,n}$ as a function of n for selected values of λ_s and λ_e. From this figure, both the even and odd behavior as well as the dramatic variations in the (λ_s, λ_e) plane can be more clearly appreciated.

The behavior of $\mathcal{N}_{n+1,n}$ in Fig. 13 is exacerbated close to the special points $\lambda_{s(e)} = \pi/2$. For instance, in the vicinity of $\lambda_s = \pi/2$, the dynamics is nondivisible even for infinites-

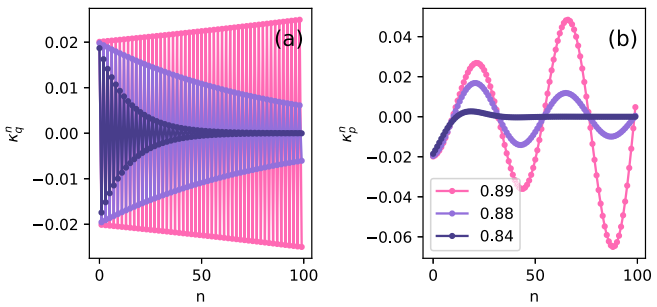

FIG. 11. Similar to Fig. 8, but for values of ν_e close to, and larger than, $\nu_e^{\text{crit}} = 0.8813$.

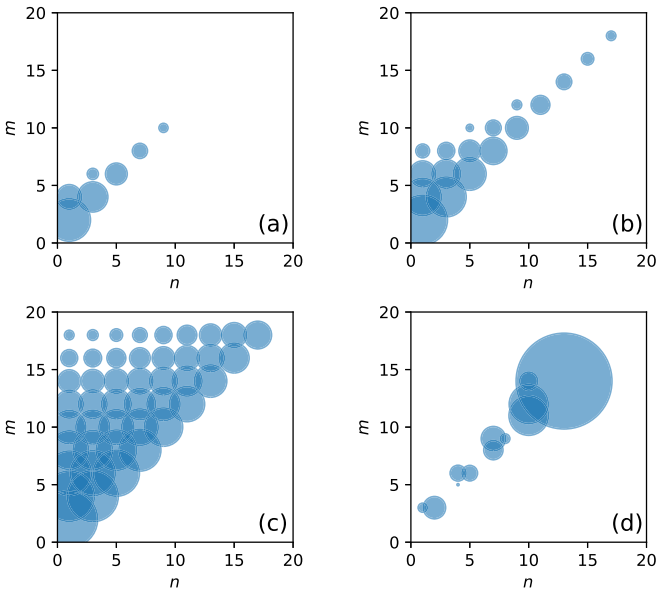

FIG. 12. Example of the divisibility criteria for the BS dynamics. The plots show $\mathcal{N}_{mn}$ in the (n, m) plane, with the size of each point reflecting the magnitude of $\mathcal{N}_{mn}$. All curves are for $\lambda_s = 1.1$ and (a) $\lambda_e = 0.75$, (b) 0.9, (c) 1.1, and (d) -0.7.

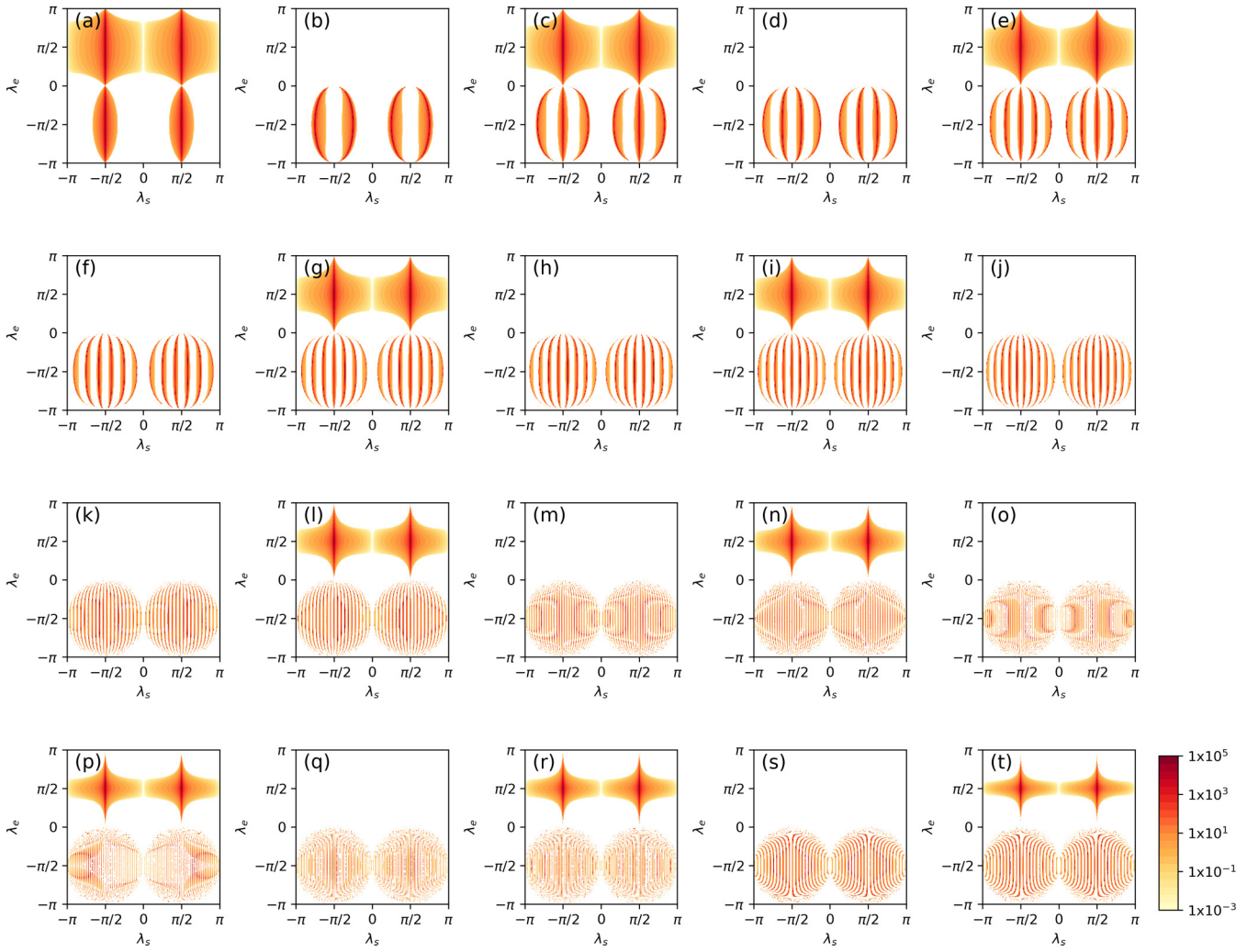

FIG. 13. CP-divisibility measure $\mathcal{N}_{n+1,n}$ [Eq. (58)] in the (λ_s, λ_e) plane, for the BS dynamics. Each plot corresponds to a different value of n: in the first two lines, n ranges from 1 to 10 in steps of 1. In the third and fourth lines, $n = 20, 21, 30, 31, 40, 41, 50,51$ and $100, 101$.

imally small λ_e. This occurs because $\lambda_s = \pi/2$ corresponds to the full SWAP, where the CM of the system is completely transferred to the ancilla. As a consequence, when the next ancilla arrives to interact with the system, it will always contain a significant amount of information about it. We therefore expect that in the limit $n \to \infty$ the diagrams in Fig. 13 should converge to narrow lines going through these special points (although, unfortunately, we cannot actually verify this since the simulation cost becomes prohibitive for extremely large n).

We may also study similar diagrams for collisions that are more broadly spaced in time. In Fig. 15 we present results for $\mathcal{N}_{1,1+m}$ for different values of m (we focus on even values, $m = 2, 4, \ldots$). This therefore describes the long-term memory of the map, concerning the first collision. Two features stand out from this figure. First, as one would expect, the overall region in the (λ_s, λ_e) plane where the map is CP divisible tends to shrink with increasing m. However, the regions around $\lambda_s = \pm\pi/2$ tend to be remarkably persistent, remaining highly nondivisible even for large m.

The results in Figs. 13 and 15 refer to divisibility for specific times (n, m). We can also combine all data and ask for which regions in the (λ_s, λ_e) plane the BS dynamics is divisible for all (n, m). This is shown in Fig. 16. As expected, for most choices of parameters, the map will not be CP divisible for some (n, m). Notwithstanding, there are regions where the map is always divisible. These regions tend to be concentrated close to $\lambda_e = 0$ (or $\lambda_e = \pi$, which is equivalent). And they exist even for large values of λ_s.

A direct comparison with the memory kernel, Sec. IV, is not generally possible since both refer to different physical aspects of the problem. But if we focus on $\mathcal{N}_{n+1,n}$, then some comparison is possible. Recall that the MK describes how the dynamics from $n \to n+1$ is affected by previous times. Thus, regions where the memory kernel is large tend to be accompanied by regions where $\mathcal{N}_{n+1,n} > 0$. This is indeed the case, as can be seen by comparing Fig. 13 with Fig. 6.

B. TMS dynamics

The situation for the TMS dynamics is dramatically different. Diagrams for $\mathcal{N}_{n+1,n}$ in the (λ_s, ν_e) plane are shown in Fig. 17 for different values of n. In contrast to the BS maps, now most of the parameter space is nondivisible. Moreover,

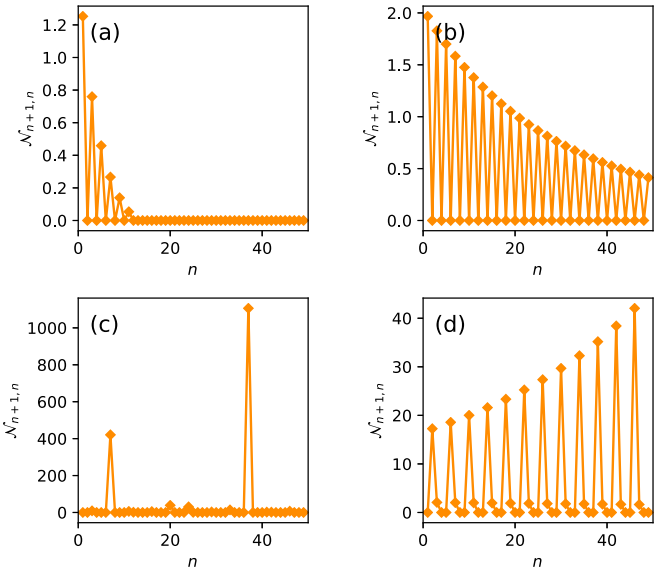

FIG. 14. CP divisibility measure $\mathcal{N}_{n+1,n}$ as a function of n, for the BS dynamics with $\lambda_s = 0.8$ and $\lambda_e = 0.9, 1.3, -0.5, -0.8$. Complements Fig. 13.

the region where it is nondivisible increases for longer times. And finally, what is perhaps the least intuitive, the regions where the map is nondivisible are denser for *small*, instead of large, ν_e (although the values of $\mathcal{N}_{n+1,n}$ are correspondingly smaller). This is a consequence of the fact that the TMS dynamics spontaneously creates excitations in the system, which implies that for large ν_e a substantial amount of noise is introduced, making the map more likely to be divisible. If $\nu_e = 0$ the map is, of course, divisible by construction. However, the results in Fig. 17 show that for arbitrarily small but nonzero ν_e the map is already nondivisible, albeit with a small $\mathcal{N}_{n+1,n}$. As with the BS dynamics, one could also combine all these diagrams to ask whether there are regions in the (λ_s, ν_e) where the map is always divisible, for all (n, m).

The answer to this question is, in this case, negative: For the TMS dynamics the dynamics is never divisible, except for the trivial line $\nu_e = 0$. This represents a major difference in comparison with the BS dynamics and, once again, is ultimately a property of the entangling nature of the two-mode squeezing interaction (13).

VI. DISCUSSION

A. Summary of main results

The goal of this paper was to provide a robust framework for studying non-Markovianity from multiple angles. We did this using two main ingredients: first, collisional models, which allow us to introduce non-Markovianity in a fully controllable way (Sec. II), and, second, continuous-variable Gaussian operations, which replace the (generally complicated) dynamics of the density matrix into a much simpler map for the covariance matrix (Sec. III). We showed that the non-Markovian dynamics can be fully encapsulated into a Markovian embedding, from which all relevant properties and quantifiers can be neatly derived. In order to gain physical insight into what is, generally, a very complicated problem, our exposition was example oriented. We focused on two types of interactions, with very distinct physical properties. Our framework, however, is general. The main results can be summarized as follows: First, concerning the general results laid down in Sec. II, we have the following.

(A1) The full non-Markovian dynamics is captured by the map $\Phi(\cdot)$ in Eq. (4) for the state ϱ^n, and the dynamics it generates, Eq. (5). At each instant of time, the reduced state of the system is always available by tracing over the ancilla.

(A2) The state ϱ^n contains all the relevant information to characterize system-environment correlations, such as the mutual information in Eq. (7).

(A3) The memory kernel can be constructed in terms of the reduced map (6) using Eq. (9).

(A4) CP divisibility can be studied using the intermediate maps $\mathcal{E}_{m\to n}$, Eq. (10).

Next, specializing this to the case of Gaussian states and processes, we have the following.

(B1) The global evolution at the level of the density matrix [Eq. (2)] is converted into an equation for the global covariance matrix [Eq. (15)]. Unitaries are replaced by symplectic matrices.

(B2) The dynamics is fully captured by the covariance matrix γ^n in Eq. (23), representing the joint state of S and E_{n+1} at time n.

(B3) The dynamics of γ^n is now Markovian and obeys the standard Gaussian CP map (24) (Markovian embedding). The matrices X, Y are related to the entries of the symplectic matrices S_n and $S_{n+1,n}$ according to Eqs. (19), (20), and (26).

(B4) The mutual information (7) is computed from the symplectic eigenvalues of γ^n.

(B5) The time-non-local dynamics defining the memory kernel, Eq. (1), can be rewritten at the level of the system covariance matrix as in (29). The memory kernel depends *only* on the matrix X and can be computed using Eq. (45). One can also write a Kraus decomposition of the MK, Eq. (29). The coefficients κ_{ij}^n are found from Eq. (48).

(B6) The intermediate map, taking the system from time n to time m, is given by Eqs. (56) and (57). A monotone of CP divisibility is given by Eq. (58) and depends only on the matrices X and Y.

All methods described above are implemented in the associated PYTHON library, which provides an efficient and simple way of simulating a broad range of scenarios. All plots presented in this paper were generated with this code and are freely available in Ref. [67].

B. Main conclusions for the BS and TMS dynamics

We have focused on two types of maps. The system-ancilla interaction was always fixed to be of beam splitter type (partial SWAP). But the ancilla-ancilla interaction could be either beam splitter or a two-mode squeezing. The behaviors of the two are dramatically different.

For the former, we have found that the combination of the two beam-splitter interactions leads to strong resonance effects that cause most quantities to oscillate in time and also depend sensibly on the relative signs of the interaction strengths (see Figs. 6 or 13). For the BS

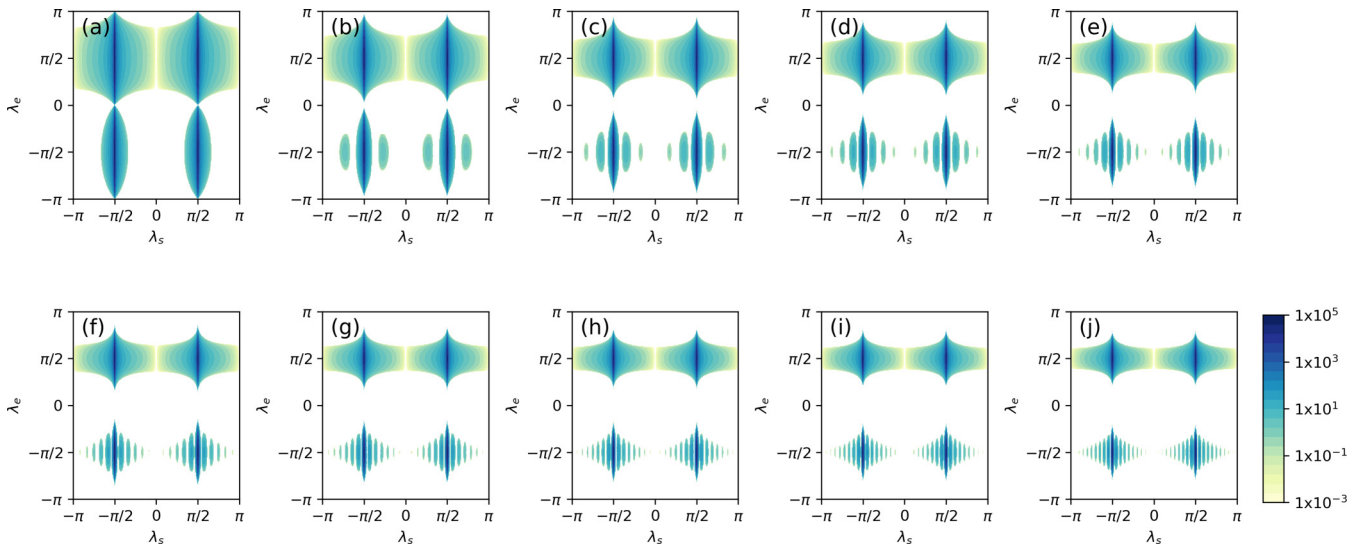

FIG. 15. CP-divisibility measure, $\mathcal{N}_{m,1}$ [Eq. (58)] in the (λ_s, λ_e) plane, for the BS dynamics. Each plot corresponds to a different value of m, from $m = 2$ to 30 in steps of 2.

dynamics, there is also a non-negligible portion of parameter space in which the dynamics is always Markovian (Fig. 16).

Conversely, in the TMS dynamics excitations are constantly being generated in the system. As a consequence, the dynamics is only stable for certain values of the interaction strength [Fig. 2(d)]. If the interaction is too strong, the occupations in the system diverge (never reach a steady state). Interestingly, this is also reflected in the memory kernel, which acquires infinitely long memory (Fig. 11). The TMS dynamics is also always non-Markovian (never CP divisible; see Fig. 17), unless the ancilla-ancilla interaction is strictly zero. This reflects the entangling nature of the two-mode squeezing. The magnitude of the non-Markovianity, of course, is small for weak interactions. This is clearly seen, for instance, in the memory kernel, Fig. 9.

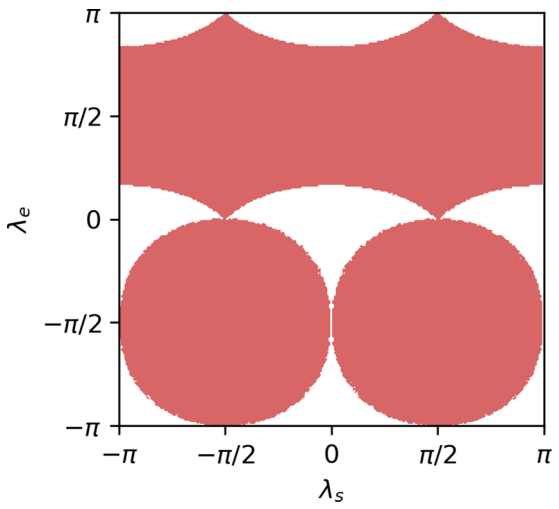

FIG. 16. Regions in the (λ_s, λ_e) plane where the BS dynamics is *not* CP divisible for at least one choice of (n, m).

C. Connection with experimentally relevant scenarios

At first, the collisional model setup may seem like an artificial description of open quantum dynamics. However, this is not so, for the following reasons. First, collisional models actually faithfully describe some experimentally relevant situations, for instance when a system is coupled to a one-dimensional (1D) waveguide [75–78]. The dispersion relation of 1D waveguides allows one to discretize the field operator into time bins, so that the interaction at each time interval only involves one bin operator. The picture that emerges is then exactly that of a collisional model. Moreover, this model is in general non-Markovian by construction, which depends on the input state of the electromagnetic field, as well as on the nature of the interaction. The specific conditions determining whether the ensuing dynamics will be Markovian or not are discussed in detail in a recent review on the subject [79].

Second, collisional models are motivated by Boltzmann's *Stosszahlansatz* (molecular chaos hypothesis) [80]. We often use baths of harmonic oscillators to model open dynamics (e.g., in Caldeira-Leggett's model [81,82]). But these are actually the ones that are artificial, since real baths are highly chaotic and ergodic, involving highly nonlinear interactions. The *Stosszahlansatz*, and hence collisional models, capture precisely this idea. At each instant of time, only a small part of the environment (the "ancilla") is actually interacting with the system. And afterwards, this part leaves and "returns to the bath," where it will collide with the other bath units and eventually thermalize, forgetting all information about the system. This is why, in collisional models, the ancillas are discarded after each collision, and fresh new ones are introduced. When they return to the bath, however, the ancillas will in general transmit information of the system to the other bath units, which is the ingredient used in this paper to introduce the non-Markovianity.

Finally, we also mention that any potential artificiality in a collisional model is actually *intentional*. The models are artificial precisely so that they can strip away many of the difficulties that may arise in real-life, uncontrolled, models.

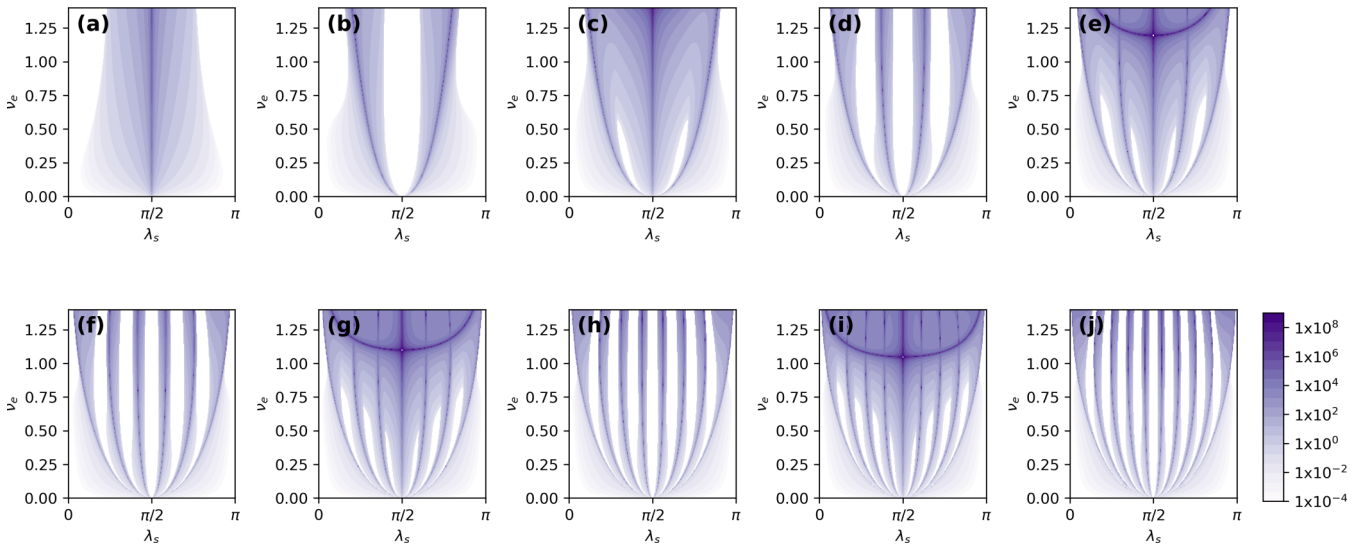

FIG. 17. CP-divisibility measure, $\mathcal{N}_{n+1,n}$ [Eq. (58)] in the (λ_s, ν_e) plane, for the TMS dynamics. Each plot corresponds to a different value of n, from 1 to 10 in steps of 1.

This kind of approach is common in physics. For instance, one may draw a parallel with ultracold atoms in optical lattices [83–85]. These systems were originally developed to mimic condensed matter systems and explain phenomena such as high-temperature superconductivity. Their motivation lay in the fact that actual solids are extremely complicated, making it difficult to pinpoint the actual mechanisms behind superconductivity. Ultracold atoms strip away these difficulties, by focusing on an artificial model, but one that contains precisely the relevant ingredients (e.g., the Fermi-Hubbard model). Artificiality is thus an advantage, not a limitation.

D. Connection with standard bosonic baths

A common configuration to study non-Markovianity is to consider a single mode a coupled to N bosonic modes $b_1, \ldots, b_N$, all at the same time. For instance, a typical Hamiltonian would be of the form

$$H = \omega a^\dagger a + \sum_{i=1}^{N} \Omega_i b_i^\dagger b_i + \sum_i g_i (a^\dagger b_i + b_i^\dagger a). \tag{59}$$

Or one could also have a quadrature-quadrature coupling of the form $(a + a^\dagger)(b + b^\dagger)$, as in the Caldeira-Leggett model [81,82]. In this section, we briefly compare the main advantages of using a collisional setup and, in particular, the Markovian embedding, versus this standard approach based on Eq. (59).

There are two main advantages, one computational and one conceptual. The computational advantage is straightforward: Even for Gaussian interactions, in order to properly account for the full evolution of a Hamiltonian such as (59), one needs to keep track of the full covariance matrix of the $N + 1$ modes involved, which will evolve according to the Lyapunov equation [58]

$$\frac{d\sigma}{dt} = \Omega H \sigma + \sigma (\Omega H)^{\mathrm{T}}, \tag{60}$$

where Ω is the symplectic form. This CM would be of size $2(N + 1)$. While this is an enormous upgrade when compared with the exponential complexity of the full Hilbert space, it can still become prohibitive if one is interested in large sizes, and especially in large times. The Markovian embedding approach, on the other hand, reduces this to the evolution of a 4×4 matrix, the size of which is independent of the number of collisions involved.

As for conceptual advantages, the defining feature, distinguishing the collisional approach from the standard one, is the ability to keep track of which specific events generate the information backflow. For instance, as argued in Sec. II B, understanding the correlations between the system and different parts of the bath is a natural way of understanding the pathways to information backflow. But for a Hamiltonian such as (59), the system will become correlated to all modes and at no specific time order. The collisional approach introduces a definite causal structure: the system interacts with one ancilla, which only afterwards propagates this to the next step. This makes it possible to pinpoint which correlations, at which times, are the relevant ones. Similar advantages are also encountered when dealing with the memory kernel or CP divisibility. For instance, explicitly constructing the memory kernel for a map such as (60) is quite complicated and involves generally extremely large matrices. But for collisional models this becomes quite tractable, as shown in Sec. IV.

E. Possible extensions

Our framework can be readily extended to a broad range of scenarios. We being by mentioning problems which are straightforward extensions of our results. Throughout the paper, we have focused on ancillas initially prepared in the vacuum state. Studying different initial preparations would be interesting since the memory kernel does not depend on this, but CP divisibility does. It would be particularly interesting to study the introduction of single-mode squeezing in the ancillas.

Another natural extension would be to consider different types of interactions, as in Refs [52,56]. In particular, one thing that we have not explored are interactions that lead to "nondiagonal" memory kernels. As discussed below Eq. (29), a MK involving the identity or σ_z is always diagonal, meaning that each entry of θ^n is only affected by the same entry at past times. A memory kernel involving $\sigma_\pm$, however, would imply, for instance, that $\langle Q^2\rangle_n$ could be affected by past values of $\langle P^2\rangle_n$. This could, in principle, generate a plethora of interesting effects. Another possibility would be the inclusion of stochastic SWAPs, as in Refs. [49,50].

In Ref. [57], the authors asked, within a collisional model context, whether it was possible to pinpoint the backflow of information to either changes in the environmental states or the buildup of correlations between system and environment. This question is relevant since these are the two main ingredients entering in the second law of thermodynamics in the quantum domain [86,87]. That is to say, they are the two quantities measuring the degree of irreversibility of a process. We believe that this question could be directly addressed within our framework. Whether the Markovian embedding suffices for this end, however, is not clear at the moment. For instance, the mutual information studied in Sec. III D is only between S and E_{n+1} and thus corresponds to only a part of the full system-environment correlations. Notwithstanding, even if the embedding does not suffice, the fact that the approach deals only with covariance matrices still allows one to study numerically dynamics involving large numbers of ancillas.

Concerning less trivial extensions, throughout this paper we have assumed that the Markov memory length is 1. That is, each ancilla E_n only propagates information to its nearest neighbor. The extension to arbitrary memory length, as studied in Refs. [52,56], would be quite interesting. And it is also amenable to our framework, provided one extends the Markovian embedding to have longer memory.

Finally, we mention that the basic ideas set up in this paper could also serve as a starting point for exploring the Gaussian formulation of process tensors [29–31], which provide an alternative, and much broader, way of characterizing non-Markovianity. In fact, this could perhaps also be used as a way to bridge process tensors and the memory kernel.

ACKNOWLEDGMENTS

The authors acknowledge fruitful discussions with S. Campbell, C. B. Maria, K. Modi. M. Frana, N. Bernardes, M. Paternostro, F. Ciccarello, and B. S. de Mendona. We particular thank S. Campbell, for also sharing simulation code for Gaussian models. G.T.L. acknowledges the São Paulo Research Foundation (Grants No. 2017/07973-5, No. 2017/50304-7, and No. 2018/12813-0). G.T.L. acknowledges the hospitality of Apt44, where part of this work was developed. R.R.C. acknowledges the Brazilian funding agency CNPq (Grant No. 157168/2018-2).

APPENDIX A: STABILITY THEORY

We are interested in studying the fixed-point stability of the Markovian embedding equation (24), i.e., solutions that satisfy $\gamma^{n+1} = \gamma^n$. To this end, we use the vectorized form (36) and label the vectorized fixed-point solution as $\vec{\gamma}^*$:

$$\vec{\gamma}^* = X \otimes X \vec{\gamma}^* + \vec{Y}. \tag{A1}$$

As long as $\det(\mathbb{I} - X \otimes X) \neq 0$ a fixed-point solution can be readily found as

$$\vec{\gamma}^* = (\mathbb{I} - X \otimes X)^{-1} \vec{Y}. \tag{A2}$$

The stability of $\vec{\gamma}^*$ will be associated to the eigenvalues of the $X \otimes X$ matrix or, what is equivalent, the eigenvalues of X. If their moduli are below 1, the fixed point will be a globally asymptotic state (GAS) and all trajectories will converge to γ^* for large enough n. Otherwise, it may diverge.

The eigenvalues of the matrix X for the BS channel, Eq. (25), read

$$\tfrac{1}{2}(-wx + x \pm \sqrt{(w+1)^2x^2 + 4wy^2}). \tag{A3}$$

Using the (λ_s, λ_e) parametrization, one finds that the only values not satisfying the GAS conditions are $\lambda_e = \pm\pi/2$ or $\lambda_s = 0, \pi$, which represent, respectively, the case where no particles flow to the ancillas and when the system does not interact at all. Excluding those points, the fixed point is a GAS given by

$$\gamma^*_{\mathrm{BS}} = \begin{pmatrix} \epsilon & 0 \\ 0 & \epsilon \end{pmatrix}. \tag{A4}$$

That is, the map tends to homogenize the system to the same initial state of the ancillas. This, of course, is what is expected of a beam-splitter or partial SWAP dynamics. It is notwithstanding interesting that it remains true even in the case of ancilla-ancilla interactions and non-Markovian dynamics.

Similarly, the eigenvalues of X for the TMS case, Eq. (27), read

$$\begin{aligned} &\tfrac{1}{2}[(1+\tilde{w})x \pm \sqrt{(\tilde{w}-1)^2x^2 - 4\tilde{w}y^2}], \\ &\tfrac{1}{2}[(1-\tilde{w})x \pm \sqrt{(\tilde{w}+1)^2x^2 + 4\tilde{w}y^2}]. \end{aligned} \tag{A5}$$

These eigenvalues only fulfill the GAS requirements in the interval where $\nu_e \in [0, \sinh^{-1}(1)]$. This therefore defines the critical value $\nu_e^{\mathrm{crit}} = \sinh^{-1}(1)$, after which the dynamics diverges. Inside this interval, the fixed point is a GAS given by

$$\gamma^*_{\mathrm{TMS}} = \begin{pmatrix} \left(\frac{2\sinh^2(\nu_e)}{1-\sinh^2(\nu_e)} + 1\right)\epsilon & 0 \\ 0 & \left(\frac{2\sinh^2(\nu_e)}{1-\sinh^2(\nu_e)} + 1\right)\epsilon \end{pmatrix}. \tag{A6}$$

Thus, we see that system and ancilla once again tend to homogenize. However, the ancilla initial state ϵ is now amplified by a factor which is always larger than unity and diverges when $\nu_e = \nu_e^{\mathrm{crit}}$. We also call attention to the fact that γ^*_{TMS} is a product state, so that no correlations survive in the long-time limit.

APPENDIX B: MEMORY KERNEL FOR THE BS DYNAMICS

In this Appendix we discuss how to obtain a more compact expression for the memory kernel (29), in the case of the BS dynamics. This case is simpler because the only nonzero coefficient is κ^n_{11}, which is proportional to the identity map.

That is to say, in this case the MK is actually just a c number, instead of a superoperator.

To accomplish this, we exploit in more detail the tensor structure of the matrices used in Sec. IV (now all specialized to $N_S = N_E = 1$). We being by noting that the matrix X of the BS dynamics, Eq. (25), can also be written as

$$X = \chi \otimes \mathbb{I}, \qquad \chi = \begin{pmatrix} x & y \\ yw & -xw \end{pmatrix}, \tag{B1}$$

where χ is now a simple 2×2 matrix and, in this Appendix, $\mathbb{I}$ will always refer to the identity of dimension 2. Similarly, the projection operator P_S in Eq. (37) can be written as

$$P_S = p_s \otimes \mathbb{I}, \qquad p_s = \begin{pmatrix} 1 & 0 \\ 0 & 0 \end{pmatrix}. \tag{B2}$$

Thus, the matrix P in Eq. (38) becomes

$$P = p_s \otimes \mathbb{I} \otimes p_s \otimes \mathbb{I}. \tag{B3}$$

This type of tensor structure, favoring slots 1 and 3, is simply a consequence of the vectorization procedure, Eq. (35).

The matrix p_s can be further decomposed as

$$p_s = |0\rangle\langle 0|, \qquad |0\rangle = \begin{pmatrix} 1 \\ 0 \end{pmatrix}. \tag{B4}$$

Dirac's notation is introduced here just for clarity; the state $|0\rangle$ is completely unrelated to the actual Hilbert-space basis of the system. The advantage of this decomposition is that it allows us to write the isometry π, in Eq. (43), as

$$\pi = \langle 0| \otimes \mathbb{I} \otimes \langle 0| \otimes \mathbb{I}. \tag{B5}$$

This now clearly shows that π contracts slots 1 and 3, while acting trivially on 2 and 4.

At this point, it is convenient to simplify the notation and introduce indices 1,2,3,4, to indicate on which slot of the tensor product the operators act. Thus, for instance, we will henceforth write

$$X \otimes X = \chi \otimes \mathbb{I} \otimes \chi \otimes \mathbb{I} := \chi_1 \chi_3, \tag{B6}$$

meaning χ_1 acts on slot 1 and χ_3 acts on slot 3. Similarly, $P = p_s^1 p_s^3$ and, therefore, $Q = 1 - p_s^1 p_s^3 := Q_{13}$ is a matrix acting only on slots 1 and 3 (we emphasize that Q_{13} cannot be written as a simple product of an operator acting on 1 and another acting on 3). Notice how the special structure appearing in Eq. (B6) is unique of the BS dynamics. For other types of dynamics, $X \otimes X$ would in general act nontrivially on all four slots. Due to this simplification, the quantity appearing inside $\pi(\ldots)\pi^{\mathrm{T}}$ in Eq. (45) will be an operator acting only on slots 1 and 3.

Next we turn to Eq. (48), describing the coefficients κ_{ij}^n. The contraction $\pi(\ldots)\pi^{\mathrm{T}}$ eliminates slots 1 and 3, so that $(M_j^{\mathrm{T}} \otimes M_i^{\mathrm{T}})$ is effectively multiplying matrices from slots 2 and 4. Thus, one may equivalently write

$$\left(M_j^{\mathrm{T}} \otimes M_i^{\mathrm{T}}\right)\pi(\ldots)\pi^{\mathrm{T}} = \pi\left[\left(\mathbb{I} \otimes M_j^{\mathrm{T}} \otimes \mathbb{I} \otimes M_i^{\mathrm{T}}\right)\ldots\right]\pi^{\mathrm{T}},$$

where $(\ldots)$ refers to all terms inside $\pi(\ldots)\pi^{\mathrm{T}}$ in Eq. (45). But from the arguments above, these quantities act only on slots 1 and 3. Combining this with the fact that $\mathrm{tr}(A \otimes B) = \mathrm{tr}(A)\mathrm{tr}(B)$ explains why, in the BS case, the only nontrivial coefficient will be κ_{11}^n, corresponding to $M_i = M_j = \mathbb{I}$. This coefficient may then be written as

$$\kappa_{11}^n = \mathrm{tr}_{13}\left\{\pi_{13}[\chi_1\chi_3(Q_{13}\chi_1\chi_3Q_{13})^n\chi_1\chi_3]\pi_{13}^{\mathrm{T}}\right\},$$

where the remaining trace is now only over slots 1 and 3. Finally, we use Eq. (B5) to express π in terms of $\langle 0|$. This allows us to write

$$\kappa_{11}^n = \langle 00|\,\bar{\chi}\,(\bar{Q}\,\bar{\chi}\,\bar{Q})^n\,\bar{\chi}\,|00\rangle, \tag{B7}$$

where $|00\rangle = |0\rangle \otimes |0\rangle$, $\bar{\chi} = \chi \otimes \chi$, and $\bar{Q} = \mathbb{I}_4 - p_s \otimes p_s$ are all objects of dimension 4. Equation (B7) therefore provides a compact representation of the memory kernel for the BS dynamics. It is expressed solely in terms of $|0\rangle$, χ, and p_s, [Eqs. (B1) and (B4)]. And it requires exponentiating only operators of dimension 4, in comparison with (45), which would have dimension 16.

[1] J. Doob, *Stochastic Processes*, Wiley Publications in Statistics (Wiley, New York, 1990).

[2] F. C. Binder, J. Thompson, and M. Gu, Phys. Rev. Lett. **120**, 240502 (2018).

[3] Á. Rivas, S. F. Huelga, and M. B. Plenio, Rep. Prog. Phys. **77**, 094001 (2014).

[4] H.-P. Breuer, E.-M. Laine, J. Piilo, and B. Vacchini, Rev. Mod. Phys. **88**, 021002 (2016).

[5] H.-P. Breuer, E.-M. Laine, and J. Piilo, Phys. Rev. Lett. **103**, 210401 (2009).

[6] D. Chruściński, Á. Rivas, and E. Størmer, Phys. Rev. Lett. **121**, 080407 (2018).

[7] R. Vasile, S. Maniscalco, M. G. A. Paris, H.-P. Breuer, and J. Piilo, Phys. Rev. A **84**, 052118 (2011).

[8] E.-M. Laine, J. Piilo, and H.-P. Breuer, Phys. Rev. A **81**, 062115 (2010).

[9] Á. Rivas, S. F. Huelga, and M. B. Plenio, Phys. Rev. Lett. **105**, 050403 (2010).

[10] S. C. Hou, X. X. Yi, S. X. Yu, and C. H. Oh, Phys. Rev. A **83**, 062115 (2011).

[11] S. Luo, S. Fu, and H. Song, Phys. Rev. A **86**, 044101 (2012).

[12] D. Chruściński and A. Kossakowski, J. Phys. B **45**, 154002 (2012).

[13] D. Chruściński and A. Kossakowski, Eur. Phys. J. D **68**, 7 (2014).

[14] A. C. S. Costa, R. M. Angelo, and M. W. Beims, Phys. Rev. A **90**, 012322 (2014).

[15] P. Strasberg and M. Esposito, Phys. Rev. Lett. **121**, 040601 (2018).

[16] L. A. M. Souza, H. S. Dhar, M. N. Bera, P. Liuzzo-Scorpo, and G. Adesso, Phys. Rev. A **92**, 052122 (2015).

[17] F. F. Fanchini, G. Karpat, B. Çakmak, L. K. Castelano, G. H. Aguilar, O. J. Farías, S. P. Walborn, P. H. Souto Ribeiro, and M. C. de Oliveira, Phys. Rev. Lett. **112**, 210402 (2014).

[18] X.-M. Lu, X. Wang, and C. P. Sun, Phys. Rev. A **82**, 042103 (2010).

[19] S. Nakajima, Prog. Theor. Phys. **20**, 948 (1958).
[20] R. Zwanzig, J. Chem. Phys. **33**, 1338 (1960).
[21] S. M. Barnett and S. Stenholm, Phys. Rev. A **64**, 033808 (2001).
[22] A. Shabani and D. A. Lidar, Phys. Rev. A **71**, 020101(R) (2005).
[23] M. J. W. Hall, J. D. Cresser, L. Li, and E. Andersson, Phys. Rev. A **89**, 042120 (2014).
[24] L. Mazzola, E. M. Laine, H. P. Breuer, S. Maniscalco, and J. Piilo, Phys. Rev. A **81**, 062120 (2010).
[25] F. Liu, X. Zhou, and Z. W. Zhou, Phys. Rev. A **99**, 052119 (2019).
[26] B. Vacchini, Phys. Rev. Lett. **117**, 230401 (2016).
[27] J. Cerrillo and J. Cao, Phys. Rev. Lett. **112**, 110401 (2014).
[28] F. A. Pollock and K. Modi, Quantum **2**, 76 (2018).
[29] F. A. Pollock, C. Rodríguez-Rosario, T. Frauenheim, M. Paternostro, and K. Modi, Phys. Rev. Lett. **120**, 040405 (2018).
[30] F. A. Pollock, C. Rodríguez-Rosario, T. Frauenheim, M. Paternostro, and K. Modi, Phys. Rev. A **97**, 012127 (2018).
[31] P. Taranto, S. Milz, F. A. Pollock, and K. Modi, Phys. Rev. A **99**, 042108 (2019).
[32] J. Rau, Phys. Rev. **129**, 1880 (1963).
[33] V. Scarani, M. Ziman, P. Štelmachovič, N. Gisin, and V. Bužek, Phys. Rev. Lett. **88**, 097905 (2002).
[34] M. Ziman, P. Štelmachovič, V. Buzžek, M. Hillery, V. Scarani, and N. Gisin, Phys. Rev. A **65**, 042105 (2002).
[35] B.-G. Englert and G. Morigi, in *Coherent Evolution in Noisy Environments*, Lecture Notes in Physics, edited by A. Buchleitner and K. Hornberger (Springer-Verlag, Berlin, 2002), p. 611.
[36] S. Attal and Y. Pautrat, Ann. Inst. Henri Poincare **7**, 59 (2006).
[37] C. Pellegrini and F. Petruccione, J. Phys. A: Math. Theor. **42**, 425304 (2009).
[38] D. Karevski and T. Platini, Phys. Rev. Lett. **102**, 207207 (2009).
[39] G. T. Landi, E. Novais, M. J. de Oliveira, and D. Karevski, Phys. Rev. E **90**, 042142 (2014).
[40] V. Giovannetti and G. M. Palma, Phys. Rev. Lett. **108**, 040401 (2012).
[41] P. Strasberg, G. Schaller, T. Brandes, and M. Esposito, Phys. Rev. X **7**, 021003 (2017).
[42] F. Barra, Sci. Rep. **5**, 14873 (2015).
[43] G. De Chiara, G. Landi, A. Hewgill, B. Reid, A. Ferraro, A. J. Roncaglia, and M. Antezza, New J. Phys. **20**, 113024 (2018).
[44] T. Rybár, S. N. Filippov, M. Ziman, and V. Bužek, J. Phys. B **45**, 154006 (2012).
[45] N. K. Bernardes, A. R. R. Carvalho, C. H. Monken, and M. F. Santos, Phys. Rev. A **90**, 032111 (2014).
[46] N. K. Bernardes, A. R. R. Carvalho, C. H. Monken, and M. F. Santos, Phys. Rev. A **95**, 032117 (2017).
[47] E. Mascarenhas and I. de Vega, Phys. Rev. A **96**, 062117 (2017).
[48] Z.-X. Man, Y.-J. Xia, and R. Lo Franco, Phys. Rev. A **97**, 062104 (2018).
[49] F. Ciccarello, G. M. Palma, and V. Giovannetti, Phys. Rev. A **87**, 040103(R) (2013).
[50] F. Ciccarello and V. Giovannetti, Phys. Scr. **2013**, 014010 (2013).
[51] R. McCloskey and M. Paternostro, Phys. Rev. A **89**, 052120 (2014).
[52] B. Çakmak, M. Pezzutto, M. Paternostro, and Ö. E. Müstecaplıoğlu, Phys. Rev. A **96**, 022109 (2017).
[53] S. Kretschmer, K. Luoma, and W. T. Strunz, Phys. Rev. A **94**, 012106 (2016).
[54] S. Campbell, F. Ciccarello, G. M. Palma, and B. Vacchini, Phys. Rev. A **98**, 012142 (2018).
[55] S. Lorenzo, F. Ciccarello, and G. M. Palma, Phys. Rev. A **96**, 032107 (2017).
[56] J. Jin and C.-S. Yu, New J. Phys. **20**, 053026 (2018).
[57] S. Campbell, M. Popovic, D. Tamascelli, and B. Vacchini, New J. Phys. **21**, 053036 (2019).
[58] A. Serafini, *Quantum Continuous Variables: A Primer of Theoretical Methods* (CRC, Boca Raton, FL, 2017).
[59] A. Ferraro, S. Olivares, and M. G. Paris, arXiv:quant-ph/0503237 (2005).
[60] G. Adesso and F. Illuminati, J. Phys. A: Math. Theor. **40**, 7821 (2007).
[61] G. Adesso, S. Ragy, and A. R. Lee, Open Systems & Information Dynamics **21**, 1440001 (2014).
[62] A. S. Holevo, Probl. Inf. Transm. **43**, 1 (2007).
[63] F. Caruso, V. Giovannetti, and A. S. Holevo, New J. Phys. **8**, 310 (2006).
[64] R. Simon, E. C. G. Sudarshan, and N. Mukunda, Phys. Rev. A **36**, 3868 (1987).
[65] R. Simon, E. C. G. Sudarshan, and N. Mukunda, Phys. Rev. A **37**, 3028 (1988).
[66] R. Simon, N. Mukunda, and B. Dutta, Phys. Rev. A **49**, 1567 (1994).
[67] The code repository, together with the simulation data, can be found at https://github.com/gtlandi/gaussianonmark.
[68] In principle one could also interpret G_n as being part of the memory kernel. However, we have opted not to do so, since G_n refers only to the states of the ancillas, while the actual dependence on the state of the system, which is what one expects from a memory kernel to model, is fully contained in $\mathcal{K}_n$.
[69] K. Kraus, *States, Effects, and Operations: Fundamental Notions of Quantum Theory*, edited by A. Böhm, J. D. Dollard, and W. H. Wooters (Springer-Verlag, Heidelberg, 1983), p. 154.
[70] M. A. Nielsen and I. L. Chuang, *Quantum Computation and Quantum Information* (Cambridge University, Cambridge, England, 2000).
[71] D. A. Turkington, *Generalized Vectorization, Cross-Products, and Matrix Calculus* (Cambridge University, Cambridge, England, 2013), p. 275.
[72] G. Torre, W. Roga, and F. Illuminati, Phys. Rev. Lett. **115**, 070401 (2015).
[73] P. Liuzzo-Scorpo, W. Roga, L. A. M. Souza, N. K. Bernardes, and G. Adesso, Phys. Rev. Lett. **118**, 050401 (2017).
[74] G. Lindblad, J. Phys. A: Math. Gen. **33**, 5059 (2000).
[75] J. A. Gross, C. M. Caves, G. J. Milburn, and J. Combes, Quantum Sci. Technol. **3**, 024005 (2018).
[76] F. Ciccarello, Quantum Measurements and Quantum Metrology **4**, 53 (2017).
[77] K. A. Fischer, R. Trivedi, V. Ramasesh, I. Siddiqi, and J. Vučković, Quantum **2**, 69 (2018).
[78] H. Pichler and P. Zoller, Phys. Rev. Lett. **116**, 093601 (2016).
[79] D. Cilluffo, A. Carollo, S. Lorenzo, J. A. Gross, G. M. Palma, and F. Ciccarello, Phys. Rev. Research **2**, 043070 (2020).
[80] J. L. Doob, in *Selected Papers on Noise and Stochastic Processes*, edited by N. Wax (Dover, New York, 1954).
[81] A. O. Caldeira and A. Leggett, Phys. Rev. Lett. **46**, 211 (1981).
[82] A. O. Caldeira, *An Introduction to Macroscopic Quantum*

Phenomena and Quantum Dissipation, 1st ed. (Cambridge University, Cambridge, England, 2014), p. 294.
[83] M. Greiner, O. Mandel, T. Esslinger, T. W. Hänsch, and I. Bloch, Nature (London) **415**, 39 (2002).
[84] I. Bloch, Nat. Phys. **1**, 23 (2005).
[85] C. Gross and I. Bloch, Science **357**, 995 (2017).
[86] M. Esposito, K. Lindenberg, and C. Van den Broeck, New J. Phys. **12**, 013013 (2010).
[87] A. M. Timpanaro, J. P. Santos, and G. T. Landi, Phys. Rev. Lett. **124**, 240601 (2020).